# Blastocyst trophectoderm endocytic activation, a marker of adverse developmental programming

Laura Caetano[1], Judith J. Eckert[2], David Johnston[3], David S. Chatelet[3], David A. Tumbarello[4], Neil R. Smyth[1], Sue Ingamells[5], Anthony Price[5] and Tom P. Fleming[1] *

[1] *Biological Sciences, Southampton General Hospital, University of Southampton, Southampton SO16 6YD, UK.*

[2] *Human Development and Health, Southampton General Hospital, University of Southampton, Southampton SO16 6YD, UK*

[3] *Biomedical Imaging Unit, Southampton General Hospital, University of Southampton, Southampton SO16 6YD, UK*

[4] *Biological Sciences, Life Sciences Building 85, University of Southampton, Southampton SO17 1BJ, UK*

[5]*Wessex Fertility Clinic, Southampton SO15 5QS*

*Correspondence address. Tel: +44-7833 048158; E-mail: t.p.fleming@soton.ac.uk

**Short title:** Blastocyst trophectoderm endocytic activation

**Keywords:** Trophectoderm, mouse blastocyst, human blastocyst, endocytosis, lysosomes, TFEB

**Words:** 6405 (excluding references and figure legends and tables)

## Abstract

**The mouse preimplantation embryo is sensitive to its environment including maternal dietary protein restriction which can alter the developmental programme and affect lifetime health. Previously, we have shown maternal low protein diet (LPD) causes reduction in blastocyst mTORC1 signalling coinciding with reduced availability of branched-chain amino acids (BCAAs) in surrounding uterine fluid. BCAA deficiency leads to increased endocytosis and lysosome biogenesis in blastocyst trophectoderm (TE), a response to promote compensatory histotrophic nutrition. Here, we first investigated the induction mechanism by individual variation in BCAA deficiency in an *in vitro* quantitative model of TE responsiveness. We found isoleucine (ILE) deficiency as the most effective activator of TE endocytosis and lysosome biogenesis, with less potent roles for other BCAAs and insulin; cell volume was also influential. TE response to low ILE included upregulation of vesicles comprising megalin receptor and cathepsin-B and the response was activated from blastocyst formation. Second, we identified the transcription factor TFEB as mediating the histotrophic response by translocation from cytoplasm to nucleus during ILE deficiency and in response to mTORC1 inhibition. Lastly, we investigated whether a similar mechanism responsive to maternal nutritional status was found in human blastocysts. Blastocysts from women with high body-mass index, but not the method of fertilisation, revealed stimulated lysosome biogenesis and TFEB nuclear migration. We propose TE lysosomal phenotype as an early biomarker of environmental nutrient stress that may associate with long-term health outcome.**

## Introduction

The preimplantation embryo can sense the levels of maternal tract nutrients in vivo and adjust its phenotype and its developmental programme to match these conditions and so aid survival. Thus, maternal dietary protein restriction induces the mouse blastocyst to upregulate trophectoderm proliferation, endocytosis, and subsequent cellular motility and invasiveness at implantation, leading to increased placental efficiency, a combination of adaptations protecting development and offspring competitiveness (Coan, et al. 2011, Eckert, et al. 2012, Sun, et al. 2014, Watkins, et al. 2015). However, whilst nutrient sensing derived from poor maternal diet may activate early compensatory responses, these also associate with later life chronic disease risk of offspring across impaired growth, cardiometabolic and neurological morbidities (Gould, et al. 2018, Lanham, et al. 2020, Watkins, et al. 2011, Watkins, et al. 2008). A similar sensitivity has been identified in the human preimplantation embryo with respect to culture environment and assisted reproductive treatment (ART) affecting development and postnatal growth and disease risk (Feuer and Rinaudo 2016, Kleijkers, et al. 2016, Sunde, et al. 2016). Thus, the early mammalian embryo is recognised as a vulnerable developmental stage in the concept known as 'Developmental Origin of Health and Disease' (DOHaD) (Fleming, et al. 2018, Hanson and Gluckman 2014).

Our previous work has concerned the induction of nutrient sensing in the mouse blastocyst given its importance across lifetime health. We found maternal low protein diet (LPD) from conception caused branched-chain amino acid (BCAA) levels (leucine, LEU; isoleucine, ILE; valine, VAL) to become depleted within the uterine fluid at the time of blastocyst formation; this coincided with reduced insulin concentration in maternal serum, all before implantation occurred (Eckert, et al. 2012). The dietary decrease in metabolites resulted in a reduction in blastocyst mammalian target of rapamycin complex 1 (mTORC1)

growth-regulating signalling (Takahara, et al. 2020) through the S6-kinase pathway (Eckert, et al. 2012) and an increase in trophectoderm (TE) endocytosis and lysosome biogenesis mediated through cytoskeletal reorganisation regulated by Rho-GTPase (Sun, et al. 2014). The endocytosis response likely represents increased histotrophic nutrition of tract proteins and lipids to combat poor maternal nutrition. Moreover, the endocytic response could be induced in vitro by culture of control embryos in medium with deficient albumin or, more specifically, deficient in BCAAs to mimic the LPD uterine fluid but with all other amino acids at levels found in normal-fed dams (NPD) (Sun, et al. 2014). More extensive manipulations of mouse embryo culture environment have demonstrated the combination of low BCAAs with low insulin levels were sufficient to induce the altered growth and cardiovascular disease phenotype in later life (Velazquez, et al. 2018).

In the current study, we further analyse the environmental responsiveness of mouse TE to identify more precisely the extracellular conditions required to induce enhanced endocytosis and lysosome biogenesis, its timing of induction during cleavage, and the mechanism regulating the cytoplasmic restructuring involved. We also conducted a preliminary investigation of whether a similar TE endocytic/lysosomal phenotype occurs in the human blastocyst (donated to research from ART) with respect to maternal metabolic condition. Collectively, our data provides new insight into the conditions causing adverse reprogramming of early development with biological and clinical implications.

## Materials and Methods

### *Animals and embryo collection*

MF1 outbred mice, kept under UK Home Office Project license and local ethics approval, were bred in-house (University of Southampton Biomedical Research Facility) in accordance

98 with the Animals (Scientific Procedures) Act of 1986 and associated Codes of Practise on a
99 07:00-19:00 h light cycle fed with standard chow. Virgin females (7-9 weeks) were naturally
100 mated overnight with MF1 males (2-6 months) and plug positive females were housed
101 individually the following morning. Mated dams were at E0.5 at 14.00 h on the day the
102 vaginal plug was detected. Two-cell embryos were flushed from the oviducts at E1.5 with H6
103 medium with 4 mg/ml BSA (H6+BSA) (Watkins, et al. 2007) after cervical dislocation and
104 dissection of the reproductive tract.
105
106 ***In vitro culture***
107 Collected 2-cell embryos were pooled and allocated to culture medium to the blastocyst stage
108 to investigate quantitatively which components of the depleted BCAA and insulin
109 composition found in LPD dams were most effective in inducing the enhanced endocytosis
110 and lysosome biogenesis phenotype found in LPD blastocysts (Eckert et al, 2012; Sun et al,
111 2014). Embryos at the 2-cell stage were cultured in defined potassium simplex optimized
112 medium (KSOM medium) in the absence of BSA but with variable amino acid (AA)
113 composition (Velazquez, et al. 2018), checked for osmolarity (250-260 mOsm) and used
114 under mineral oil at 37°C in 5% $CO_2$ until the morula or blastocyst stage of development,
115 depending on experimental design. Control medium consisted of KSOM supplemented with
116 insulin (1 ng/ml) (ThermoFisher) and the complete amino acid composition as previously
117 found in the MF1 uterine luminal fluid of dams at E3.5 fed a normal protein diet (**Table 1**)
118 (Eckert, et al. 2012). This included the BCAAs valine (0.46 mM), isoleucine (0.21 mM) and
119 leucine (0.32 mM). In experimental treatment groups, a combination or individual BCAA
120 concentration was decreased (50%, L-) compared with control (100%, N-BCAA) whilst all
121 other AA concentrations remained unchanged. Also, insulin was included at normal (N-INS,
122 1 ng/ml) or decreased by 50% (L-INS). All AAs were sourced from Sigma.

***Endocytosis assay***

After culture, embryos at E3.5 had reached the blastocyst stage and were incubated for 1 hour in the same medium but containing Self-Quenched BODIPY FL Conjugate of BSA (BSA-BODIPY, 0.5 mg/ml) (BioVision) and LysoTracker Red DND-99 (100 nM) (ThermoFisher) or Magic Red™ (Bio-Rad) to label degraded protein after endocytosis, lysosomes and Cathepsin B, respectively. After incubation, embryos were washed 3 times in H6+BSA and fixed in 1% formaldehyde in PBS for 20 minutes. After fixation, embryos were also washed in PBS 3 times and labelled with the plasma membrane stain CellMask™ Deep Red (Thermo Fisher Scientific) for 1 h at room temperature (1:200 in PBS) to label trophectoderm (TE) cell boundaries. At that stage, embryos were either stained with 0.2 µg/ml DAPI (Invitrogen), washed 3 times in Tween-20 (Sigma-Aldrich) 1:1000 in PBS (PBS-T) and mounted with 20 µl Citifluor or underwent immunocytochemistry.

***Rapamycin treatment***

2-cell stage embryos (E1.5) were cultured after collection in N-BCAA/N-INS medium (**Table 1**) supplemented with rapamycin (LC laboratories, Woburn, USA) at final concentrations of 100 nM, 1 µM or 20 µM at 37°C in 5% $CO_2$. After 36 hours in culture, embryos were transferred to fresh medium containing the same concentration of rapamycin until reaching the blastocyst stage. Control embryos were cultured in KSOM without rapamycin but complemented with DMSO at 1:1000 (rapamycin solvent). At that point, embryos were stained with LysoTracker, fixed in 1% formaldehyde in PBS for 20 minutes and imaged by confocal microscopy before immunocytochemistry.

***Immunocytochemistry***

Antibodies used for immunolabelling were: rabbit polyclonal anti transcription factor EB (TFEB) gene 7942 (A303-673A-T Bethyl Laboratories; 1:50); mouse monoclonal to megalin (Protein G purified, 1:400) (Meads and Wild 1993); and rabbit polyclonal anti-clathrin (Cell Signaling P1663, 1:400). Secondary antibodies were: Alexa 546, 488 and 633 (Invitrogen; 1:300). Negative controls were included by omitting the primary antibody. Embryos, previously fixed and stained with CellMask, were subsequently permeabilised with 0.25% Triton-X-100 (Sigma-Aldrich) in PBS (PBS-T) for 15 minutes, washed in PBS-T and neutralised in 2.6 mg/ml $NH_4Cl$ (Sigma-Aldrich) in PBS for 10 minutes. Embryos were then washed 3 times (5 minutes each) in PBS-T before incubation with primary antibody (diluted in PBS-T) overnight at 4°C. The following day, embryos were washed with PBS-T (3 times for 10 minutes each), incubated with secondary antibody for 1 h at room temperature, washed in PBS-T (3 times for 10 minutes), nuclear stained with DAPI (Invitrogen; 0.2 μg/ml in PBS-T; 20 mins), washed 3 times in PBS-T and mounted with 20 μl Citifluor.

***Confocal microscopy, image capture and analysis***

Embryos were viewed with a Leica SP5 confocal microscope. Images were acquired by accumulation of z-series of TE cells on the surface closest to the coverslip, 50-60 xy sections at 0.15 μm intervals, tangential to the embryo surface and extending from apical to basal surfaces of examined TE cells to provide a high resolution dataset. Images from confocal microscopy were analysed with VOLOCITY-3D 6.3 quantification software (PerkinElmer). Measurements were made in individual TE cells with 1-3 adjacent TE cells analysed per embryo. A VOLOCITY protocol was designed for each individual labelling method used based on vesicle/structure sizes and applied to all embryos in different treatment groups. The optimised protocol is provided in **Supplementary Table 1.** Using these settings, VOLOCITY was used to calculate number and volume of labelled vesicles per TE cell and to

measure the distance from the vesicles centre to the nucleus edge. VOLOCITY was also used to measure cell volume as required.

***Human embryo study***

Vitrified embryos were donated with full patient consent for research under HFEA licence from Wessex Fertility Clinic, Southampton. Donors were selected based upon maternal BMI (two groups, normal 18.9-22.9; high >25; 27.1-32.3); patient age (less than 38); embryo number per patient (minimum 3); embryo stage (all vitrified from day (D) 3 or later). The normal and high BMI patient groups and embryos analysed are shown in **Table 2**. Vitrified embryos were thawed with Vit Kit®-Thaw 90137-SO (Irvine Scientific) for 5 minutes at 37°C in 40 µl drop of thawing solution in a 4-well dish under sterile conditions on heated stage. Embryos were then transferred to the kit's dilution solution at room temperature for 4 minutes followed by 2 x 4-minute washes in washing solution at room temperature. Embryos were then transferred singly into pre-equilibrated drops (40 µl) of Sage 1-step™ medium with HSA and phenol red (Origio) in a 6 cm dish covered with mineral oil (Origio) and incubated at 37°C with 5% $CO_2$ and 5% $O_2$ to develop to blastocyst stage at D5. At this stage, embryos were incubated with LysoTracker (as used for mouse embryos but omitting BSA-BODIPY co-labelling), fixed and immunolabelled with TFEB (as for mouse embryos).

***Statistical analysis***

Mouse embryo data were first assessed for normality using the Shapiro–Wilk normality test. Data analysis was performed using One-Way ANOVA and Tukey's post hoc test for multi comparisons or Student's t-test for normally distributed data (~75% samples); and with Kruskal-Wallis test with Dunn's multiple comparisons post hoc test or Mann-Whitney for non-normally distributed data (~25% samples). Pooling data across experiments to increase

sample number showed lysosome number per cell to be normally distributed, and analysis of our non-normalised data by tests for normalised data did not alter statistical significance. Human embryo lysosome biogenesis and immunocytochemistry data were assessed using the multilevel random effects regression model (SPSS version 25) which takes into account potential hierarchical nature of the data with between-patient and within-patient variation and different parameters measured from individual embryos. Thus, differences identified between groups studied are independent of cell volume, cell number and whether a resultant pregnancy occurred from a sibling embryo collected at the same time. Data are presented as dot plots and, for mouse, with box and whisker markers to identify the median and interquartile range and min/max points with $P<0.05$ regarded as significant.

## Results

### *A role for isoleucine in activating mouse embryo endocytosis and lysosome biogenesis*

Our first experiments were to identify the relative role of deficiency of the three BCAAs, leucine (LEU), isoleucine (ILE) and valine (VAL), shown previously to enhance endocytosis and lysosome biogenesis in trophectoderm (TE) in our diet and in vitro models (Eckert, et al. 2012, Sun, et al. 2014) and whether deficient insulin was contributory. Control 2-cell embryos were cultured to blastocyst stage (~48 h) in KSOM medium with the complete uterine fluid composition of AAs (**Table 1**) and systemic insulin (1 ng/ml) as found in NPD-fed dams (N-BCAA/N-INS). In tested culture medium, one of three BCAAs was individually reduced by 50% compared to the NPD uterine fluid concentration and normal insulin (L-VAL/N-INS; L-LEU/N-INS; L-ILE/N-INS), or normal concentration of BCAAs but 50% decreased insulin (N-BCAA/L-INS). Blastocysts were examined for endocytosis and

lysosomes using combined BSA-BODIPY and LysoTracker assay by confocal microscopy and image analysis.

In all groups, LysoTracker and BSA-BODIPY labelled vesicles were mainly co-localised around the TE nucleus, viewed *en face*, tangential to the coverslip (**Figure 1A**) with data accrued from high resolution z-series across the complete cell layer. Blastocysts in the L-ILE/N-INS group had increased number and collective volume of BSA-BODIPY positive vesicles per cell (P=0.04, 0.03 respectively) while LysoTracker number and collective volume per cell were increased but not significantly (P=0.09 and 0.06, respectively) (**Figure 1B-E**) compared to the control N-BCAA/N-INS. L-ILE/N-INS was also increased in BSA-BODIPY vesicle number compared to L-VAL/N-INS (P=0.017) and N-BCAA/L-INS (P=0.014) and in collective volume of vesicles in N-BCAA/L-INS P=0.05) (**Figure 1C,E**). L-ILE/N-INS LysoTracker vesicle number and collective volume was increased compared with N-BCAA/L-INS P=0.02 and 0.02 respectively) **(Figure 1B,D)**. In contrast, L-VAL/N-INS, L-LEU/N-INS and N-BCAA/L-INS were not different in vesicle labelling from the N-BCAA/N-INS controls although L-LEU/N-INS mean or median values for all analyses were above those of other groups except L-ILE/N-INS, a larger dataset would be required to expose any effect (**Figure 1B-D**). Further analysis showed that the increase in L-ILE/N-INS vesicle dynamics was not caused by increased vesicle size compared to controls indicating endocytosis and lysosome enhancement were by collective increase in vesicle number (**Supplemental Figure 1A,B**). The average distance of both vesicles (BSA-BODIPY and LysoTracker) to the nucleus was not altered across treatments (**Supplemental Figure 1C,D**). Lastly, all treatments resulted in a consistent blastocyst formation rate of ~70% and with equivalent cell numbers present (**Supplemental Figure 1E,F**) indicating these treatments did not affect embryo viability, as found for later treatments. Collectively, these data indicate

247 embryo endocytosis and lysosomes were increased in response to reduced isoleucine (L-ILE)
248 alone in the culture medium, a partial response may be induced by low leucine (L-LEU),
249 while valine and insulin deficiency produced no effect.
250
251 To determine whether increased LysoTracker vesicle number and collective volume per
252 cell in the L-ILE/N-INS group reflected an actual increase in lysosomal enzyme activity,
253 blastocysts from this treatment were also assayed with Magic Red staining which fluoresces
254 in response to cleavage by the lysosome enzyme, Cathepsin B (**Figure 2A**). In the L-ILE/N-
255 INS group, Magic Red staining was increased in terms of collective vesicle volume per TE
256 cell (P=0.04) but the increase for vesicle number per cell was not significant (P=0.1)
257 compared to the N-BCAA/N-INS control (**Figure 2B,C***).*
258
259 To investigate whether endocytosis upregulation in response to L-ILE/N-INS coincided
260 with increased expression of endocytic receptor, megalin, and endocytic vesicle coat protein,
261 clathrin, these proteins were analysed by immunocytochemistry (**Figure 2D-G**). Both
262 megalin and clathrin were concentrated along the apical surface of TE cells as well as within
263 vesicles in the apical cytoplasm (**Figure 2D,E**). Megalin (P=0.02) and clathrin (P=0.002)
264 signal intensities were increased in L-ILE/N-INS blastocyst TE cells when compared to the
265 N-BCAA/N-INS control using standardised settings for fluorescent intensity by total voxel
266 count per channel (**Figure 2F,G***).*
267
268 ***Combinations of depleted BCAAs and/or insulin can activate embryo endocytosis***
269 To further examine individual and combined BCAA interactions with insulin, embryos were
270 collected at E1.5 (2-cell stage) and cultured until blastocyst stage (~48 h) in six KSOM media
271 treatments: N-BCAA/N-INS (control), L-ILE/N-INS (positive control from above), L-ILE/L-

INS, L-LEU/L-INS, L-ILE/L-LEU/L-INS and L-BCAA/L-INS (**Figure 3A**). An increase in BSA-BODIPY collective vesicle volume per cell (P=0.04) and vesicle number per cell (P=0.07) was present in the L-ILE/N-INS positive control. Increased BSA-BODIPY vesicle number and collective vesicle volume per cell were also present in the L-ILE/L-LEU/L-INS combination treatment (P=0.002 and 0.005 respectively) (**Figure 3B-E**). Collective volume of BSA-BODIPY vesicles per cell was higher but not significant in the L-BCAA/L-INS group (P=0.09). Other L-INS groups show a consistent non-significant increase in mean BSA-BODIPY vesicle number and collective volume per cell compared with the N-BCAA/N-INS control. Similarly, LysoTracker vesicle number and collective volume per cell were increased in all combination treatments compared with control N-BCAA/N-INS but not to statistical significance (**Figure 3B-E***)*. In all six culture treatments, individual size of vesicles did not differ (**Supplemental Figure 2A,B***)* indicating changes in collective volume where present reflected an increase in vesicle number. The mean distance of both vesicles to the nucleus was also not altered by treatment (**Supplemental Figure 2C,D**). Collectively, these data suggest minor stimulatory effects on endocytosis and lysosomes may be mediated by some combined metabolite combinations. The effect of L-ILE deficiency alone was the focus of future mouse experiments.

***Stimulation of lysosome biogenesis by low isoleucine activates at the blastocyst stage***

Embryos were collected at E1.5 (2-cell stage) and cultured until the morula stage (36 h; ~16-cell stage) in KSOM medium with L-ILE/N-INS or in control medium (N-BCAA/N-INS). At the morula stage, embryos were examined using the LysoTracker assay alongside blastocysts (cultured for 48 h) used as a positive control (**Figure 4A**). Embryos cultured until the morula stage in L-ILE/N-INS group had no change in LysoTracker vesicle number or collective volume per cell compared to the N-BCAA/N-INS control group while blastocyst lysosome

297 number (P=0.002) or collective volume (P=0.06) were enhanced (**Figure 4B-E**). Note,
298 morula vesicle number/cell is about double that of the blastocyst reflecting larger cell volume
299 at the morula 16-cell stage. Collectively, these data indicate that the capacity for lysosome
300 biogenesis initiates at the blastocyst stage.
301
302 ***Isoleucine deficiency activates TFEB nuclear translocation in blastocyst TE cells***
303 We next considered further downstream regulation of enhanced endocytosis and lysosome
304 biogenesis following induction by isoleucine deficiency. The transcription factor TFEB has
305 been shown to interact with mTORC1 on lysosomal membranes and upon reduction in
306 mTORC1 signalling is translocated to the nucleus and increases transcription of multiple
307 genes implicated in lysosomal biosynthesis and autophagy (Sardiello, et al. 2009, Settembre,
308 et al. 2012). TFEB subcellular localization was analysed in blastocysts after culture from 2-
309 cell stage in either L-ILE/N-INS or N-BCAA/N-INS (**Figure 5A**). To quantify cellular
310 localisation, the relative volumes of TFEB in the cytoplasm and nucleus in TE cells were
311 ratioed. TFEB switched from an approximate equal cytoplasmic / nuclear (~50:50%)
312 localisation in N-BCAA/N-INS to a predominant nuclear localisation (~20:80 cytoplasmic /
313 nuclear) (P=0.02) in L-ILE/N-INS culture (**Figure 5B,C***)*. Pearson Correlation was used with
314 VOLOCITY software to calculate the relative association between green (TFEB) and blue
315 (DAPI) channels and showed TFEB was localised more in the nucleus in L-ILE/N-INS
316 (P=0.02) compared to N-BCAA/N-INS (**Figure 5D**).
317
318 ***TFEB localisation in blastocysts is sensitive to mTORC1***
319 Embryos were collected at E1.5 (2-cell stage) and cultured in control N-BCAA/N-INS
320 medium supplemented with rapamycin to inhibit mTORC1 signalling at different
321 concentrations (1 μM or 20 μM) or without rapamycin. At the blastocyst stage, embryos were

assessed for TFEB localisation (**Figure 6A**) as previously described or were analysed in the same medium using the LysoTracker assay (**Figure 7**). Rapamycin (20 μM) caused a dramatic translocation of TFEB from cytoplasm to nucleus (P=0.0001) confirmed using Pearson Correlation analysis (P=0.0001) with an intermediate effect evident at lower dose (1 μM; P=0.04) (**Figure 6B,C**). However, no significant difference was found in LysoTracker staining between the three groups although an increase in collective volume of lysosomes was detected at 20 μM rapamycin (P=0.06) (**Figure 7B**). These data first confirm that TFEB nuclear localisation in our model is regulated by loss of mTORC1 signalling, and there is evidence that mTORC1 may promote increased lysosome biogenesis.

***Effect of cell volume on endocytosis and lysosome biogenesis***

To understand whether the increase in endocytosis and lysosome biogenesis following L-ILE/N-INS culture was superimposed upon more general cellular mechanism(s) affecting the number or density of these organelles in relation to the cell cycle and division (Carlton, et al. 2020), the VOLOCITY software was used to measure cell volume using the same samples as reported above. No difference was found in blastocyst TE cell volume in relation to control and experimental treatments with deficient individual BCAAs or INS (**Figure 8A**). The relationship between cell volume and BSA-BODIPY or LysoTracker vesicle numbers was further explored through correlation analysis following control (N-BCAA/N-INS) and L-ILE/N-INS treatments. LysoTracker vesicle number and collective volume per cell in both treatments were positively correlated with cell volume (N-BCAA/N-INS P=0.0004 and P=0.0006 respectively; L-ILE/N-INS P=0.02 for both) (**Figure 8B,C**). However, BSA-BODIPY vesicle number and collective volume per cell were only significantly positively correlated with cell volume in the L-ILE/N-INS group (P=0.01 and P=0.0009 respectively) (**Figure 8D,E**). Notably, the data indicate that the L-ILE/N-INS sample points and best-fit

lines (red) lie above those for N-BCAA/N-INS (blue) indicating L-ILE/N-INS to be stimulatory independent of cell volume. However, some L-ILE/N-INS data points show both high vesicle number or volume combined with high cell volume indicating these factors can be associated.

The N-BCAA/N-INS and L-ILE/N-INS treatments did not affect cell volume in those samples analysed for TFEB localisation (**Figure 8F**) but here, following correlation analysis, no correlation between TFEB % nuclear staining and cell volume was apparent (**Figure 8G**). Collectively, these results indicate first that while cell volume is similar across treatments, it nevertheless has a general treatment-independent positive effect upon endocytosis and lysosomes. Second, L-ILE/N-INS treatment can enhance endocytosis and lysosome biogenesis both independent of cell volume but also in association with it.

***Activation of lysosome biogenesis in human embryos***

Embryos donated from 14 patients (7 in both normal and high BMI groups) were cultured (n=81 embryos, 42 in the normal BMI group, 39 in the high BMI group) from embryonic D3 (~8-cells) to D5 (blastocyst stage). From these, 36% and 41%, respectively, developed to blastocysts and had similar total embryo volume (P=0.88; data not shown) (**Table 2**). Thirteen blastocysts from 7 patients from the normal BMI group and 15 blastocysts from 7 patients from the high BMI group (3 embryos lost during processing) were analysed successfully using LysoTracker assay for lysosomes (**Figure 9A,B**) and subsequently for TFEB localisation using immunocytochemistry (**Figure 10**). Embryos from within the high BMI group exhibited an enhanced lysosome collective volume per cell (P=0.015), similar to that previously seen in mouse embryos, although individual embryo scores were highly variable in the high BMI group (**Figure 9A,B**). Also, embryo cell number and cell volume

were not significantly different between the BMI groups (**Figure 9C,D**) although both were influencing cofactors in the lysosome statistical analysis whilst whether patient pregnancy occurred that cycle was not a cofactor. Furthermore, examination of human embryos for TFEB localisation (**Figure 10A,B**) revealed mean nuclear versus cytoplasmic localization in the high BMI group to be higher (P=0.1) (**Figure 10B**).

The LysoTracker and TFEB results shown in the scatter plots for BMI groups also include mother number for each embryo and reveal similarity in outcome between sibling embryos from the same mother (**Figure 9B, 10B**). In addition to BMI, the dataset was also screened for whether intra-cytoplasmic sperm injection (ICSI) had been employed or not. This revealed no effect on lysosome or TFEB localisation but further show the closeness in outcomes for sibling embryos (**Figure 10C,D**). Collectively, these data indicate lysosome activity and TFEB localisation in human blastocysts is sensitive to environmental factors including patient BMI.

## Discussion

Our study centred on the functioning of the extra-embryonic trophectoderm (TE) layer, the first cell type to differentiate on the surface of the mammalian embryo. TE contributes to blastocyst morphogenesis through the timing of transepithelial transport which permits blastocoel formation and regulated nutrient and metabolite provision for the inner cell mass (ICM) comprising the entire stem cell pool for fetal development (Eckert and Fleming 2008). Nutrient provision for the embryo is also mediated by histotrophic means through maturation of a polarised apicobasal endocytic pathway with fluid-phase and receptor-mediated processing via multi-ligand megalin and cubilin receptors for internalisation of uterine fluid

proteins and lipids (Assémat, et al. 2005, Fleming and Pickering 1985, Kelleher, et al. 2019). After implantation, the TE continues its supportive function and gives rise to the chorio-allantoic placenta regulating the nutritional demands of the fetus throughout gestation. In this context, the TE requires cellular mechanisms to ascertain environment nutrient levels to sustain embryo and fetal growth through pregnancy despite variations in maternal lifestyle and diet.

Past studies using the mouse LPD model have revealed maternal LPD reduced the concentration of BCAAs within maternal serum and the uterine fluid that bathes the morula and blastocyst before implantation, coinciding with reduced systemic insulin and a decrease in blastocyst mTORC1 serine/threonine kinase signalling through reduced phosphorylation of the downstream effector, ribosomal S6 protein (Eckert, et al. 2012). TE cells within LPD blastocysts respond by increased endocytosis and lysosome formation, which we considered a histotrophic response to compensate for poor maternal nutrition (Sun, et al. 2014). TE endocytosis is known to be insulin-sensitive (Dunglison, et al. 1995) and the increased endocytosis phenotype after LPD can be mimicked by culture of control blastocysts in medium deficient in either protein or the BCAAs (LEU, ILE, VAL) (Sun, et al. 2014). A similar histotrophic mechanism is found in ovine and porcine embryos whereby uterine fluid LEU and other amino acids signal through mTORC1 in TE cells to coordinate conceptus growth (Kim, et al. 2013, Kim, et al. 2011). Moreover, increased endocytosis is a recognised cellular process outside developmental models to combat protein deprivation signalled through low BCAA availability and mTORC1 (Jones, et al. 2012).

Whilst the stimulation in TE endocytosis and lysosomes mediated through maternal LPD may compensate nutritional requirements for development, it is also an early cellular

biomarker for adverse developmental programming as LPD offspring in later life develop growth, cardiometabolic and neurological morbidities (Gould, et al. 2018, Lanham, et al. 2020, Watkins, et al. 2011, Watkins, et al. 2008), outcomes that can be induced in control embryos by culture in medium deficient in BCAA and insulin (Velazquez, et al. 2018). We consider the activation of histotrophic nutrition, along with other compensatory responses by extra-embryonic lineages to promote maternal nutrient delivery following LPD, despite protecting survival, to contribute to over-nutrition during fetal growth and a postnatal metabolism that encourages adiposity and chronic disease (discussed in (Fleming, et al. 2018, Velazquez, et al. 2019). Thus, the compensatory promotion of nutrient delivery activated by maternal LPD during preimplantation is maintained even if restricted diet is not continued beyond implantation leading to increased fetal : placental weight ratio in late gestation, offspring perinatal weight becoming positively correlated with later life disease risk, and, in female offspring, sustained overweight throughout life (Watkins, et al. 2015, Watkins, et al. 2011, Watkins, et al. 2008). The mechanisms underlying induction of the endocytosis and lysosome phenotype therefore acquire further importance in the search for protection measures against periconceptional DOHaD programming (Fleming, et al. 2018).

In our current study, we have broadly used our previous method to quantify endocytosis and lysosome formation in mouse blastocysts in vitro following culture in medium with amino acid composition matching that found within uterine fluid of control fed (NPD) dams but with deficiency in BCAAs (Sun, et al. 2014). However, we have improved the protocol by omitting the need for zona removal by transient acidic medium which may cause cellular stress to embryos, and by refining the VOLOCITY image analysis of confocal z-series to increase vesicle resolution (see Methods). Our mouse experiments concerned identification of precise environmental metabolite conditions that caused activation of the

447 endocytosis and lysosome formation phenotype and the timing and cellular signalling activity
448 involved. Collectively, our data firstly pinpoint the central role of isoleucine (ILE)
449 deficiency, with more peripheral roles for other low BCAA and insulin levels in combination,
450 as environmental factors which activate the histotrophic response in mouse TE. Second, we
451 show these culture conditions promote the endocytic phenotype only from the time of
452 blastocoel formation and involves recruitment of the TFEB transcription factor to enter the
453 nucleus, mediated through mTORC1 downregulation. Lastly, we provided evidence of a
454 similar environmental responsiveness in the human blastocyst, in this case through high
455 maternal BMI as a measure of suboptimal nutrition, leading to increased lysosomal
456 phenotype and nuclear localisation of TFEB.
457
458 The identification of a central role for extracellular ILE deficiency in activating the
459 endocytosis phenotype is unexpected. The BCAAs share a similar structure of non-linear
460 aliphatic side chains and catabolic pathway via α-keto acid formation (Shimomura, et al.
461 2006, Zhang, et al. 2017). They also share several common amino acid transporters for
462 exchange at the cell membrane (Bröer and Bröer 2017) and BCAA uptake via characterised
463 transporter systems promoting mouse blastocyst development including mTORC1 signalling
464 have been reported (Eckert, et al. 2012, Lamb and Leese 1994, Martin, et al. 2003, Van
465 Winkle, et al. 2006). However, as signalling metabolites, LEU is recognised as having a more
466 potent efficacy in stimulating mTORC1 than either ILE or VAL. BCAA activation of
467 mTORC1 is mediated through the Rag GTPases such that LEU binds to the inhibitory
468 regulator of Rags, Sestrin-2, to disrupt inhibition at higher potency than either ILE or VAL
469 (Melick and Jewell 2020, Wolfson, et al. 2016). Thus, in many examples of mTORC1
470 signalling of cellular metabolism and growth, LEU acts with greater potency than other
471 BCAAs (Tomiya, et al. 2007, Yoshizawa, et al. 2002) but in a minority of cases, ILE has

been shown a more effective upstream activator, such as in mouse models for mammary cell signalling and lactation performance (Liu, et al. 2017) and in anti-angiogenic signalling in the colon (Murata and Moriyama 2007). ILE supplementation of maternal drinking water in early mouse gestation has also been shown to affect fetal growth and birthweight (To, et al. 2020). There is also evidence that metabolic effector pathways related to mTORC1 exhibit increased sensitivity to ILE than LEU as in glucose uptake and regulation in myotubes (Doi, et al. 2003) and hepatocytes (Xiao, et al. 2014), indicating the ratio of BCAA availability to have a critical influence on mTORC1-related metabolic activity (Duan, et al. 2017). Thus, in our endocytosis and lysosome model, the central role of ILE deficiency in its activation may reflect reduced mTORC1 signalling in combination with other metabolic factors such as glucose regulation, known to be affected in the LPD model both maternally (Eckert, et al. 2012, Kwong, et al. 2000) and in fetal offspring (Kwong, et al. 2007).

Our data further showed that the TE cellular reorganisation induced by ILE deficiency involved increased levels of apically-localised megalin receptor and clathrin endocytic components in combination with increased cathepsin B lysosomal enzyme activity, visualised by MagicRed. The response activated only from the time of blastocyst formation. This likely reflects the requirement for epithelial maturation to be complete including tight junction sealing and meaningful transepithelial transport to commence which occurs at this stage (Eckert and Fleming 2008, Fleming and Pickering 1985). The endocytic and lysosomal response to L-ILE/N-INS culture also involved the re-localisation of TFEB from mostly cytoplasmic sites to the nucleus. TFEB is a member of the MiT-TFE family of helix-loop-helix leucine-zipper transcription factors (Steingrímsson, et al. 2004). TFEB resides at the lysosome under conditions of nutrient availability in association with mTORC1 via Rab32 where it is phosphorylated and inactivated by the mTORC1 kinase; however, under

conditions of nutrient deprivation, through BCAA sensing requiring the Rag-GTPase regulator of mTORC1, TFEB is dephosphorylated and activated to translocate to nucleus to promote gene expression and lysosome biogenesis (Drizyte-Miller, et al. 2020, Puertollano, et al. 2018, Roczniak-Ferguson, et al. 2012, Settembre, et al. 2012). We also found TFEB translocation to the nucleus was induced by rapamycin even in conditions of nutrient availability (N-BCAA/N-INS) confirming nutrient sensing and response was regulated through mTORC1.

Individual cell volume was found not to differ across treatments. However, cell volume was positively correlated with endocytosis and lysosome vesicle number and collective volume in the mouse study and was also an influencing cofactor identified in the human study. Cell cycling and division induce stabilised partitioning of endo-lysosomal organelles between daughter cells in relation to cell volume via cytoskeletal means (Carlton, et al. 2020). Moreover, some cyclin-dependent kinases (CDKs) interact with lysosomes to maintain their homeostasis (Ishii, et al. 2019, Nowosad, et al. 2020). The relationship found between lysosome vesicle density and cell volume in mouse TE cells was evident in all treatments and linked to cell cycle as shown by the approximate doubling of vesicle number or collective volume in the morula (~16-cell) versus unstimulated blastocyst (~32-cell). Whilst ILE deficiency in the blastocyst raised endocytosis and lysosome vesicle density and collective volume relative to controls, this occurred across the range of cell volume indicating independence from cell volume. However, a subset of the L-ILE/N-INS data with high vesicle number or collective volume also had large cell volume, indicating cell volume to be a secondary factor associated with the lysosomal stimulation. Cell volume regulation in mouse oocytes and early cleavage embryos is mediated through glycine and glutamine acting as organic osmolytes and volume-regulated anion channels to export organic osmolytes

where necessary (Baltz and Tartia 2010, Tscherner, et al. 2021). However, since these amino acids occur at similar levels in LPD and NPD blastocysts (Eckert, et al. 2012); were present at the same concentration in all the current culture media which were checked for osmolarity (250-260 mOsm); and acceptable and equivalent developmental potential occurred in all treatments, we believe the association not to be linked with perturbation. The additional increase in nuclear localisation of TFEB in response to L-ILE/N-INS was found not to be influenced by cell volume. This likely reflects the direct control of TFEB localisation by mTORC1 activity rather than cell cycle dynamics.

From our mouse studies we therefore conclude that poor nutrient availability is sensed by the TE once it is a functional epithelium at the blastocyst stage, in particular by ILE deficiency through mTORC1 leading to nuclear translocation of TFEB to coordinate increased endocytosis and lysosome biogenesis by transcriptional reprogramming to compensate by histotrophic nutrition of uterine fluid. The mouse TE endocytosis and lysosome phenotype therefore acts as a biomarker of adversely programmed embryos, whilst better protected for survival during gestation, having increased disease risk in later life. To explore the clinical relevance of these findings, the lysosome phenotype was assessed in human embryos donated for research.

For the human embryo analysis, culture in media with differing nutrient levels was not a feasible strategy since maternal heterogeneity in demographics would have confounded the analysis. Thus, normalised culture of embryos to form blastocysts was conducted and maternal BMI (high and normal groups) was used as a proxy for distinct nutritional environments. This preliminary study revealed increased collective volume of lysosome vesicles per TE cell in the high BMI group but with clear variation evident per embryo.

547 Moreover, TFEB was distributed preferentially in the nucleus in blastocysts from high BMI
548 mothers, further indicating aspects of maternal metabolic status influence the embryo
549 phenotype. We also found that embryos from the same mother exhibited a similar lysosome
550 and TFEB staining pattern but other aspects of treatment, such as ICSI versus non-ICSI
551 fertilisation, or whether pregnancy resulted from that cycle, did not appear influential. This is
552 consistent with a similar metabolic profile occurring in embryos derived from ICSI and
553 conventional IVF (Leary and Sturmey 2020).
554
555 Whilst our evidence that maternal nutritional environment influences lysosome status
556 and TFEB distribution in the human blastocyst is limited and requires a larger study for
557 confirmation, it is consistent with deleterious effects and reduced fertility identified in
558 oocytes and embryos from obese and high BMI mothers (Machtinger, et al. 2012, van der
559 Steeg, et al. 2008). Overweight mothers generate fewer and smaller oocytes that give rise to
560 blastocysts at a reduced rate and with fewer TE cells than those of normal BMI mothers
561 (Bartolacci, et al. 2019, Comstock, et al. 2015, Leary, et al. 2015). Blastocysts from
562 overweight mothers also exhibit impaired glucose metabolism and increased triglyceride
563 content (Leary, et al. 2015) reflecting increased accumulation of metabolites within follicular
564 fluid (Robker, et al. 2009). However, in contrast to our mouse study, the altered profile of
565 lysosomes and TFEB distribution is mediated not through deficiency in immediate culture
566 composition but from maternal metabolism. In this context, our human data is more similar to
567 our maternal LPD mouse model but with dietary condition being overnutrition rather than
568 protein restriction. High maternal BMI did not significantly alter the uterine fluid
569 composition of individual amino acids but generally increased their mean concentration
570 (Kermack, et al. 2015), in contrast to their reduction in the mouse LPD model (Eckert, et al.
571 2012). A maternal diet validated as less healthy than one with reduced fats and more

572 vegetables and fruit also resulted in increased uterine fluid AAs with individual BCAAs
573 significantly increased (Kermack, et al. 2015). Interestingly, improved Mediterranean-style
574 diet has been shown to stimulate human embryo development and lead to increased
575 pregnancy over less healthy diets comprising higher fat intake (Braga, et al. 2015, Kermack,
576 et al. 2020, Vujkovic, et al. 2010). Thus, the increased lysosomal phenotype found in
577 blastocysts from the high BMI group may reflect more a stress response to over nutrition than
578 a deficiency in metabolites. Embryo screening for developmental potential in clinical ART is
579 predominantly restricted to morphological and morphokinetic approaches with limited scope
580 for embryo metabolic health (Ferrick, et al. 2020). Whilst the lysosomal phenotype of
581 adverse metabolic health revealed here depended upon invasive processing, advanced non-
582 invasive light microscopy technologies and imaging (eg, optical coherence microscopy;
583 (Karnowski, et al. 2017)) are emerging for visualisation of cytoplasmic organelles that may
584 lead to improved embryo selection.
585
586 In conclusion, we describe a critical early mechanism in mouse preimplantation
587 development to combat low maternal nutrient availability, activated especially by ILE
588 deficiency but also by depletion in other BCAAs and insulin in the blastocyst TE. This signal
589 leads to stimulation in endocytosis and lysosome biogenesis to increase compensatory
590 histotrophic nutrition mediated by reduced mTORC1 activity that promotes nuclear
591 translocation of the TFEB transcription factor. The mechanism associates with increased risk
592 of chronic disease in later life, hence is an early marker of adverse periconceptional
593 programming. In a preliminary study, a similar capacity for increased lysosome biogenesis is
594 evident in human blastocysts activated in response to high maternal BMI and, if
595 substantiated, may provide a means to assess embryo metabolic potential in a clinical setting.
596

## Declaration of interest

The authors declare that there is no conflict of interest that could be perceived as prejudicing the impartiality of the research reported.

## Funding

This work was supported through the Rosetrees Trust (A798), the Biotechnology and Biological Sciences Research Council (BBSRC) (BB/F007450/1) and the University of Southampton to TPF.

## Ethics

Mice were kept under UK Home Office Project license to T P F and local ethics approval in accordance with the Animals (Scientific Procedures) Act of 1986 and associated Codes of Practise. Human embryos were donated with consent from Wessex Fertility Clinic under a Human Fertilisation and Embryology Authority research licence to T P F and J J E.

## Author contribution statement

L C performed experiments, analysed data and wrote and edited the manuscript. J J E provided embryo and statistical expertise, analysed data and edited the manuscript. D J, D S C and N R S provided technical support and edited the manuscript. D A T provided cellular expertise and edited the manuscript. S I and A P provided human embryo access and expertise via HFEA research licence, and edited the manuscript. T P F conceived and designed the study and wrote and edited the manuscript.

## Acknowledgements

We thank staff from the University of Southampton Biomedical Research Facility for animal provision and maintenance and the Biomedical Imaging Facility for microscopy and imaging facilities.

## References

**Assémat, E, S Vinot, F Gofflot, P Linsel-Nitschke, F Illien, F Châtelet, P Verroust, S Louvet-Vallée, F Rinninger, and R Kozyraki** 2005 Expression and role of cubilin in the internalization of nutrients during the peri-implantation development of the rodent embryo. *Biol Reprod* **72** 1079-1086.

**Baltz, JM, and AP Tartia** 2010 Cell volume regulation in oocytes and early embryos: connecting physiology to successful culture media. *Hum Reprod Update* **16** 166-176.

**Bartolacci, A, J Buratini, C Moutier, MC Guglielmo, PV Novara, F Brambillasca, MM Renzini, and M Dal Canto** 2019 Maternal body mass index affects embryo morphokinetics: a time-lapse study. *J Assist Reprod Genet* **36** 1109-1116.

**Braga, DP, G Halpern, AS Setti, RC Figueira, A Iaconelli, Jr., and E Borges, Jr.** 2015 The impact of food intake and social habits on embryo quality and the likelihood of blastocyst formation. *Reprod Biomed Online* **31** 30-38.

**Bröer, S, and A Bröer** 2017 Amino acid homeostasis and signalling in mammalian cells and organisms. *Biochem J* **474** 1935-1963.

**Carlton, JG, H Jones, and US Eggert** 2020 Membrane and organelle dynamics during cell division. *Nat Rev Mol Cell Biol* **21** 151-166.

**Coan, PM, OR Vaughan, J McCarthy, C Mactier, GJ Burton, M Constancia, and AL Fowden** 2011 Dietary composition programmes placental phenotype in mice. *J Physiol* **589** 3659-3670.

**Comstock, IA, S Kim, B Behr, and RB Lathi** 2015 Increased body mass index negatively impacts blastocyst formation rate in normal responders undergoing in vitro fertilization. *J Assist Reprod Genet* **32** 1299-1304.

**Doi, M, I Yamaoka, T Fukunaga, and M Nakayama** 2003 Isoleucine, a potent plasma glucose-lowering amino acid, stimulates glucose uptake in C2C12 myotubes. *Biochem Biophys Res Commun* **312** 1111-1117.

**Drizyte-Miller, K, J Chen, H Cao, MB Schott, and MA McNiven** 2020 The small GTPase Rab32 resides on lysosomes to regulate mTORC1 signaling. *J Cell Sci* **133**.

**Duan, Y, L Zeng, F Li, W Wang, Y Li, Q Guo, Y Ji, B Tan, and Y Yin** 2017 Effect of branched-chain amino acid ratio on the proliferation, differentiation, and expression levels of key regulators involved in protein metabolism of myocytes. *Nutrition* **36** 8-16.

**Dunglison, GF, SD Jane, TF McCaul, JE Chad, TP Fleming, and PL Kaye** 1995 Stimulation of endocytosis in mouse blastocysts by insulin: a quantitative morphological analysis. *J Reprod Fertil* **105** 115-123.

**Eckert, JJ, and TP Fleming** 2008 Tight junction biogenesis during early development. *Biochim Biophys Acta* **1778** 717-728.

**Eckert, JJ, R Porter, AJ Watkins, E Burt, S Brooks, HJ Leese, PG Humpherson, IT Cameron, and TP Fleming** 2012 Metabolic induction and early responses of mouse

664 blastocyst developmental programming following maternal low protein diet affecting
665 life-long health. *PLoS One* **7** e52791.
666 **Ferrick, L, YSL Lee, and DK Gardner** 2020 Metabolic activity of human blastocysts
667 correlates with their morphokinetics, morphological grade, KIDScore and artificial
668 intelligence ranking. *Hum Reprod* **35** 2004-2016.
669 **Feuer, S, and P Rinaudo** 2016 From Embryos to Adults: A DOHaD Perspective on In Vitro
670 Fertilization and Other Assisted Reproductive Technologies. *Healthcare (Basel)* **4**.
671 **Fleming, TP, and SJ Pickering** 1985 Maturation and polarization of the endocytotic system
672 in outside blastomeres during mouse preimplantation development. *J Embryol Exp*
673 *Morphol* **89** 175-208.
674 **Fleming, TP, AJ Watkins, MA Velazquez, JC Mathers, AM Prentice, J Stephenson, M**
675 **Barker, R Saffery, CS Yajnik, JJ Eckert, et al** 2018 Origins of lifetime health
676 around the time of conception: causes and consequences. *Lancet* **391** 1842-1852.
677 **Gould, JM, PJ Smith, CJ Airey, EJ Mort, LE Airey, FDM Warricker, JE Pearson-Farr,**
678 **EC Weston, PJW Gould, OG Semmence, et al** 2018 Mouse maternal protein
679 restriction during preimplantation alone permanently alters brain neuron proportion
680 and adult short-term memory. *Proc Natl Acad Sci U S A*.
681 **Hanson, MA, and PD Gluckman** 2014 Early developmental conditioning of later health and
682 disease: physiology or pathophysiology? *Physiol Rev* **94** 1027-1076.
683 **Ishii, S, A Matsuura, and E Itakura** 2019 Identification of a factor controlling lysosomal
684 homeostasis using a novel lysosomal trafficking probe. *Sci Rep* **9** 11635.
685 **Jones, CB, EM Ott, JM Keener, M Curtiss, V Sandrin, and M Babst** 2012 Regulation of
686 membrane protein degradation by starvation-response pathways. *Traffic* **13** 468-482.
687 **Karnowski, K, A Ajduk, B Wieloch, S Tamborski, K Krawiec, M Wojtkowski, and M**
688 **Szkulmowski** 2017 Optical coherence microscopy as a novel, non-invasive method
689 for the 4D live imaging of early mammalian embryos. *Sci Rep* **7** 4165.
690 **Kelleher, AM, FJ DeMayo, and TE Spencer** 2019 Uterine Glands: Developmental Biology
691 and Functional Roles in Pregnancy. *Endocr Rev* **40** 1424-1445.
692 **Kermack, AJ, S Finn-Sell, YC Cheong, N Brook, JJ Eckert, NS Macklon, and FD**
693 **Houghton** 2015 Amino acid composition of human uterine fluid: association with
694 age, lifestyle and gynaecological pathology. *Hum Reprod* **30** 917-924.
695 **Kermack, AJ, P Lowen, SJ Wellstead, HL Fisk, M Montag, Y Cheong, C Osmond, FD**
696 **Houghton, PC Calder, and NS Macklon** 2020 Effect of a 6-week "Mediterranean"
697 dietary intervention on in vitro human embryo development: the Preconception
698 Dietary Supplements in Assisted Reproduction double-blinded randomized controlled
699 trial. *Fertil Steril* **113** 260-269.
700 **Kim, J, G Song, G Wu, H Gao, GA Johnson, and FW Bazer** 2013 Arginine, leucine, and
701 glutamine stimulate proliferation of porcine trophectoderm cells through the MTOR-
702 RPS6K-RPS6-EIF4EBP1 signal transduction pathway. *Biol Reprod* **88** 113.
703 **Kim, JY, RC Burghardt, G Wu, GA Johnson, TE Spencer, and FW Bazer** 2011 Select
704 nutrients in the ovine uterine lumen. VII. Effects of arginine, leucine, glutamine, and
705 glucose on trophectoderm cell signaling, proliferation, and migration. *Biol Reprod* **84**
706 62-69.
707 **Kleijkers, SH, E Mantikou, E Slappendel, D Consten, J van Echten-Arends, AM**
708 **Wetzels, M van Wely, LJ Smits, AP van Montfoort, S Repping, et al** 2016
709 Influence of embryo culture medium (G5 and HTF) on pregnancy and perinatal
710 outcome after IVF: a multicenter RCT. *Hum Reprod* **31** 2219-2230.
711 **Kwong, WY, DJ Miller, AP Wilkins, MS Dear, JN Wright, C Osmond, J Zhang, and TP**
712 **Fleming** 2007 Maternal low protein diet restricted to the preimplantation period

induces a gender-specific change on hepatic gene expression in rat fetuses. *Mol Reprod Dev* **74** 48-56.

**Kwong, WY, AE Wild, P Roberts, AC Willis, and TP Fleming** 2000 Maternal undernutrition during the preimplantation period of rat development causes blastocyst abnormalities and programming of postnatal hypertension. *Development* **127** 4195-4202.

**Lamb, VK, and HJ Leese** 1994 Uptake of a mixture of amino acids by mouse blastocysts. *J Reprod Fertil* **102** 169-175.

**Lanham, SA, SJ Smith, AJ Watkins, ES Lucas, N MacCaoilte, ROC Oreffo, TP Fleming, and JJ Eckert** 2020 Periconception maternal low-protein diet adversely affects male mouse fetal bone growth and mineral density quality in late gestation. *J Dev Orig Health Dis* 1-12.

**Leary, C, HJ Leese, and RG Sturmey** 2015 Human embryos from overweight and obese women display phenotypic and metabolic abnormalities. *Hum Reprod* **30** 122-132.

**Leary, C, and RG Sturmey** 2020 Metabolic profile of in vitro derived human embryos is not affected by the mode of fertilization. *Mol Hum Reprod* **26** 277-287.

**Liu, GM, MD Hanigan, XY Lin, K Zhao, FG Jiang, RR White, Y Wang, ZY Hu, and ZH Wang** 2017 Methionine, leucine, isoleucine, or threonine effects on mammary cell signaling and pup growth in lactating mice. *J Dairy Sci* **100** 4038-4050.

**Machtinger, R, CM Combelles, SA Missmer, KF Correia, JH Fox, and C Racowsky** 2012 The association between severe obesity and characteristics of failed fertilized oocytes. *Hum Reprod* **27** 3198-3207.

**Martin, PM, AE Sutherland, and LJ Van Winkle** 2003 Amino acid transport regulates blastocyst implantation. *Biol Reprod* **69** 1101-1108.

**Meads, TJ, and AE Wild** 1993 Apical expression of an antigen common to rabbit yolk sac endoderm and kidney proximal tubule epithelium. *J Reprod Immunol* **23** 247-264.

**Melick, CH, and JL Jewell** 2020 Regulation of mTORC1 by Upstream Stimuli. *Genes (Basel)* **11**.

**Murata, K, and M Moriyama** 2007 Isoleucine, an essential amino acid, prevents liver metastases of colon cancer by antiangiogenesis. *Cancer Res* **67** 3263-3268.

**Nowosad, A, P Jeannot, C Callot, J Creff, RT Perchey, C Joffre, P Codogno, S Manenti, and A Besson** 2020 p27 controls Ragulator and mTOR activity in amino acid-deprived cells to regulate the autophagy-lysosomal pathway and coordinate cell cycle and cell growth. *Nat Cell Biol* **22** 1076-1090.

**Puertollano, R, SM Ferguson, J Brugarolas, and A Ballabio** 2018 The complex relationship between TFEB transcription factor phosphorylation and subcellular localization. *EMBO J* **37**.

**Robker, RL, LK Akison, BD Bennett, PN Thrupp, LR Chura, DL Russell, M Lane, and RJ Norman** 2009 Obese women exhibit differences in ovarian metabolites, hormones, and gene expression compared with moderate-weight women. *J Clin Endocrinol Metab* **94** 1533-1540.

**Roczniak-Ferguson, A, CS Petit, F Froehlich, S Qian, J Ky, B Angarola, TC Walther, and SM Ferguson** 2012 The transcription factor TFEB links mTORC1 signaling to transcriptional control of lysosome homeostasis. *Sci Signal* **5** ra42.

**Sardiello, M, M Palmieri, A di Ronza, DL Medina, M Valenza, VA Gennarino, C Di Malta, F Donaudy, V Embrione, RS Polishchuk, et al** 2009 A gene network regulating lysosomal biogenesis and function. *Science* **325** 473-477.

**Settembre, C, R Zoncu, DL Medina, F Vetrini, S Erdin, S Erdin, T Huynh, M Ferron, G Karsenty, MC Vellard, et al** 2012 A lysosome-to-nucleus signalling mechanism senses and regulates the lysosome via mTOR and TFEB. *EMBO J* **31** 1095-1108.

**Shimomura, Y, Y Yamamoto, G Bajotto, J Sato, T Murakami, N Shimomura, H Kobayashi, and K Mawatari** 2006 Nutraceutical effects of branched-chain amino acids on skeletal muscle. *J Nutr* **136** 529s-532s.

**Steingrímsson, E, NG Copeland, and NA Jenkins** 2004 Melanocytes and the microphthalmia transcription factor network. *Annu Rev Genet* **38** 365-411.

**Sun, C, MA Velazquez, S Marfy-Smith, B Sheth, A Cox, DA Johnston, N Smyth, and TP Fleming** 2014 Mouse early extra-embryonic lineages activate compensatory endocytosis in response to poor maternal nutrition. *Development* **141** 1140-1150.

**Sunde, A, D Brison, J Dumoulin, J Harper, K Lundin, MC Magli, E Van den Abbeel, and A Veiga** 2016 Time to take human embryo culture seriously. *Hum Reprod* **31** 2174-2182.

**Takahara, T, Y Amemiya, R Sugiyama, M Maki, and H Shibata** 2020 Amino acid-dependent control of mTORC1 signaling: a variety of regulatory modes. *J Biomed Sci* **27** 87.

**To, CY, M Freeman, and LJ Van Winkle** 2020 Consumption of a Branched-Chain Amino Acid (BCAA) during Days 2-10 of Pregnancy Causes Abnormal Fetal and Placental Growth: Implications for BCAA Supplementation in Humans. *Int J Environ Res Public Health* **17**.

**Tomiya, T, T Nishikawa, Y Inoue, N Ohtomo, H Ikeda, K Tejima, N Watanabe, Y Tanoue, M Omata, and K Fujiwara** 2007 Leucine stimulates HGF production by hepatic stellate cells through mTOR pathway. *Biochem Biophys Res Commun* **358** 176-180.

**Tscherner, AK, AD Macaulay, CS Ortman, and JM Baltz** 2021 Initiation of cell volume regulation and unique cell volume regulatory mechanisms in mammalian oocytes and embryos. *J Cell Physiol*.

**Tsichlaki, E, and G FitzHarris** 2016 Nucleus downscaling in mouse embryos is regulated by cooperative developmental and geometric programs. *Sci Rep* **6** 28040.

**van der Steeg, JW, P Steures, MJ Eijkemans, JD Habbema, PG Hompes, JM Burggraaff, GJ Oosterhuis, PM Bossuyt, F van der Veen, and BW Mol** 2008 Obesity affects spontaneous pregnancy chances in subfertile, ovulatory women. *Hum Reprod* **23** 324-328.

**Van Winkle, LJ, JK Tesch, A Shah, and AL Campione** 2006 System B0,+ amino acid transport regulates the penetration stage of blastocyst implantation with possible long-term developmental consequences through adulthood. *Hum Reprod Update* **12** 145-157.

**Velazquez, MA, TP Fleming, and AJ Watkins** 2019 Periconceptional environment and the developmental origins of disease. *J Endocrinol* **242** T33-t49.

**Velazquez, MA, B Sheth, SJ Smith, JJ Eckert, C Osmond, and TP Fleming** 2018 Insulin and branched-chain amino acid depletion during mouse preimplantation embryo culture programmes body weight gain and raised blood pressure during early postnatal life. *Biochim Biophys Acta Mol Basis Dis* **1864** 590-600.

**Vujkovic, M, JH de Vries, J Lindemans, NS Macklon, PJ van der Spek, EA Steegers, and RP Steegers-Theunissen** 2010 The preconception Mediterranean dietary pattern in couples undergoing in vitro fertilization/intracytoplasmic sperm injection treatment increases the chance of pregnancy. *Fertil Steril* **94** 2096-2101.

**Watkins, AJ, ES Lucas, S Marfy-Smith, N Bates, SJ Kimber, and TP Fleming** 2015 Maternal nutrition modifies trophoblast giant cell phenotype and fetal growth in mice. *Reproduction* **149** 563-575.

**Watkins, AJ, ES Lucas, A Wilkins, FR Cagampang, and TP Fleming** 2011 Maternal periconceptional and gestational low protein diet affects mouse offspring growth, cardiovascular and adipose phenotype at 1 year of age. *PLoS One* **6** e28745.

**Watkins, AJ, D Platt, T Papenbrock, A Wilkins, JJ Eckert, WY Kwong, C Osmond, M Hanson, and TP Fleming** 2007 Mouse embryo culture induces changes in postnatal phenotype including raised systolic blood pressure. *Proc Natl Acad Sci U S A* **104** 5449-5454.

**Watkins, AJ, E Ursell, R Panton, T Papenbrock, L Hollis, C Cunningham, A Wilkins, VH Perry, B Sheth, WY Kwong, et al** 2008 Adaptive responses by mouse early embryos to maternal diet protect fetal growth but predispose to adult onset disease. *Biol Reprod* **78** 299-306.

**Wolfson, RL, L Chantranupong, RA Saxton, K Shen, SM Scaria, JR Cantor, and DM Sabatini** 2016 Sestrin2 is a leucine sensor for the mTORC1 pathway. *Science* **351** 43-48.

**Xiao, F, J Yu, Y Guo, J Deng, K Li, Y Du, S Chen, J Zhu, H Sheng, and F Guo** 2014 Effects of individual branched-chain amino acids deprivation on insulin sensitivity and glucose metabolism in mice. *Metabolism* **63** 841-850.

**Yoshizawa, F, S Hirayama, H Sekizawa, T Nagasawa, and K Sugahara** 2002 Oral administration of leucine stimulates phosphorylation of 4E-bP1 and S6K 1 in skeletal muscle but not in liver of diabetic rats. *J Nutr Sci Vitaminol (Tokyo)* **48** 59-64.

**Zhang, S, X Zeng, M Ren, X Mao, and S Qiao** 2017 Novel metabolic and physiological functions of branched chain amino acids: a review. *J Anim Sci Biotechnol* **8** 10.

## Figure legends

**Figure 1.** Endocytosis and lysosomes are increased in mouse blastocyst TE following culture from 2-cell stage in medium with depleted Isoleucine alone and normal Insulin (L-ILE/N-INS). **A.** Blastocysts z-series after BSA-BODIPY (green) and LysoTracker (red) endocytosis and lysosome assay and nuclei (DAPI, blue) staining following culture in different BCAAs concentrations - either at the level found in NPD uterine fluid (N-BCAA), or with one BCAA individually reduced by 50% compared to N-BCAA (L-VAL/N-INS, L-LEU/N-INS and L-ILE/N-INS) or with normal concentration of BCAAs but 50% decreased insulin (L-INS). Scale bar = 20 μm**. B-E**. LysoTracker and BSA-BODIPY vesicle number and collective volume ($\mu m^3$) per TE cell. Endocytosis and lysosome number are stimulated in the L-ILE/N-INS group but not significantly in the other treatment groups. Data were analysed by 1-way ANOVA and shown as dot plots with box and whisker markers to identify the median and

847 interquartile range and min/max points. *P <0.05; for other P values, see text;17-24 embryos
848 per group (30-55 cells per group) from 13 mothers (in 10 replicates). Abbreviations: N-
849 BCAA/N-INS Normal BCAA, normal insulin; L-VAL/N-INS low valine, normal insulin; L-
850 LEU/N-INS low leucine, normal insulin; L-ILE/N-INS low isoleucine, normal insulin; N-
851 BCAA/L-INS normal BCAA, low insulin.
852
853 **Figure 2.** Cathepsin B (MagicRed) activity and megalin (red) and clathrin (green)
854 immunostaining are increased in mouse blastocyst TE following culture from 2-cell stage in
855 media with depleted Isoleucine (L-ILE/N-INS) **A.** Blastocysts after MagicRed (red) and
856 LysoTracker (green) assay and nuclei (DAPI, blue) staining following culture in either the
857 BCAA level found in NPD uterine fluid (N-BCAA), or with reduced (50%) Isoleucine (L-
858 ILE). **B,C.** Cathepsin B vesicle number and collective volume per TE cell is increased in the
859 L-ILE/N-INS group. 21-26 embryos per group from 7 mothers (in 4 replicates). **D.** N-
860 BCAA/N-INS and **E.** L-ILE/N-INS blastocysts stained for megalin (red), clathrin (green) and
861 nuclei (DAPI, blue). High magnification of TE layer shown below; markers are localised to
862 apical TE and cytoplasm. **F.** Megalin and **G.** Clathrin staining intensity (voxels) is increased
863 in L-ILE/N-INS blastocyst TE cells. 10-18 embryos per group from 6 mothers in 4 replicates.
864 Scale bar = 20 μm. Data were analysed by t-test (**B,C**) and Mann-Whitney (**F,G**) and shown
865 as dot plots with box and whisker markers to identify the median and interquartile range and
866 min/max points. *P < 0.05, **P < 0.01; for other P values, see text. Abbreviations: N-
867 BCAA/N-INS Normal BCAA, normal insulin; L-ILE/N-INS low isoleucine, normal insulin.
868
869 **Figure 3.** Endocytosis is increased in mouse blastocyst TE following culture from 2-cell
870 stage in media with L-ILE/N-INS and L-ILE/L-LEU/L-INS. Culture in L-BCAA/L-INS
871 increased endocytosis to a trend level. **A.** Representative blastocysts after BSA-BODIPY

872 (green) and LysoTracker (red) endocytosis assay and nuclei (DAPI, blue) staining following
873 culture in different combinations of BCAAs and insulin concentrations – BCAAs were either
874 at the level found in NPD uterine fluid (N-BCAA), with one BCAA individually reduced by
875 50% (L-ILE or L-LEU), with two BCAA reduced by 50% (L-ILE and L-LEU) or with all
876 BCAA reduced by 50% (L-BCAA) either with normal insulin (N-INS) or with 50%
877 decreased insulin (L-INS). Scale bar = 20 μm. **B,C.** LysoTracker and **D,E.** BSA-BODIPY
878 vesicles number and collective volume ($\mu m^3$) per TE cell. Endocytosis is stimulated in the L-
879 ILE/N-INS and L-ILE/L-LEU groups but not significantly in the other depleted media.
880 Embryos cultured in L-BCAA/L-INS had a trend to increase endocytosis. Data were analysed
881 by Kruskal-Wallis (**B-D**) and 1-way ANOVA (**E**) and shown as dot plots with box and
882 whisker markers to identify the median and interquartile range and min/max points. *P< 0.05,
883 **P<0.01; for other P values, see text; 13-19 embryos per group (23-38 cells per group) from
884 14 mothers (in 8 replicates). Abbreviations: N-BCAA/N-INS Normal BCAA, normal insulin;
885 L-ILE/N-INS low isoleucine, normal insulin; L-BCAA/L-INS low BCAA, low insulin; L-
886 ILE/L-INS low isoleucine, low insulin; L-LEU/L-INS low leucine, low insulin; L-ILE/L-
887 LEU/L-INS low isoleucine, low leucine, low insulin.
888
889 **Figure 4.** Lysosomes are not increased in mouse morulae outer cells following culture from
890 2-cell stage in media with depleted Isoleucine alone and normal insulin (L-ILE/N-INS). **A.**
891 Morulae after LysoTracker (LysTr, red) lysosome assay following culture in (N-BCAA/N-
892 INS; L-ILE/N-INS). Blastocysts used as control (embryos from same experiment left in
893 culture for 12h more). Scale bar = 20 μm. **B,C.** Morula LysoTracker vesicle number and
894 collective volume ($\mu m^3$) per outer cell. **D,E.** Blastocyst LysoTracker vesicle number and
895 collective volume ($\mu m^3$) per TE cell. Data were analysed by Mann-Whitney and shown as dot
896 plots with box and whisker markers to identify the median and interquartile range and

897 min/max points. **P < 0.01; for other P values, see text. 17-18 embryos per group (24-26
898 cells per group) from 5 mothers (in 4 replicates). Abbreviations: N-BCAA/N-INS Normal
899 BCAA, normal insulin; L-ILE/N-INS low isoleucine, normal insulin.
900
901 **Figure 5.** TFEB staining in N-BCAA/N-INS mouse blastocysts is more cytoplasmic while in
902 L-ILE/N-INS it is more nuclear. **A.** TFEB staining in blastocysts following culture from 2-
903 cell stage. Scale bar = 20 μm. **B,C.** Percentage (%) TFEB localised in the cytoplasm (**C**) and
904 in the nucleus (**D**). **E.** Pearson's correlation for green and blue channel. L-ILE/N-INS TE
905 cells have increased proportion of the TFEB (green channel) co-labelled with the nucleus
906 (DAPI – blue channel). Data were analysed by t-test (**B,C**) and Mann-Whitney (**D**) and
907 shown as dot plots with box and whisker markers to identify the median and interquartile
908 range and min/max points. *P < 0.05; for other P values, see text; 7-8 embryos per group (9-
909 10 cells per group) from 4 mothers (in 4 replicates). Abbreviations: N-BCAA/N-INS Normal
910 BCAA, normal insulin; L-ILE/N-INS low isoleucine, normal insulin.
911
912 **Figure 6. A.** 2-cell mouse embryos cultured until blastocyst stage in N-BCAA/N-INS
913 medium supplemented with rapamycin at different concentrations – 0 , 1 or 20 μM before
914 immunolabelling for TFEB (green) and DAPI (blue). Scale bar = 20 μm. **B.** Percentage (%)
915 TFEB localisation in nuclei rather than cytoplasm increased with Rapamycin treatment. **C.**
916 Pearson correlation showing increased co-localisation between TFEB and DAPI (nuclear
917 staining) as rapamycin concentration increases. Data were analysed by Kruskal-Wallis and
918 shown as dot plots with box and whisker markers to identify the median and interquartile
919 range and min/max points. *P< 0.05, *** P< 0.001; for other P values, see text. 6-13 embryos
920 per group from 5 mothers (in 4 replicates). Abbreviations: N-BCAA/N-INS Normal BCAA,
921 normal insulin.

**Figure 7. A.** 2-cell stage mouse embryos cultured to blastocyst stage in N-BCAA/N-INS medium supplemented with rapamycin at different concentrations, 0, 100 nm, 1 or 20 μM, before LysoTracker analysis (LysTr, red) and DAPI (blue). Scale bar = 20 μm. **B.** LysoTracker collective volume/cell is not significantly changed by rapamycin although slightly increased at 20 μM. Data were analysed by Kruskal-Wallis test and shown as dot plots with box and whisker markers to identify the median and interquartile range and min/max points. For select P values, see text; 6-13 embryos per group from 5 mothers (in 4 replicates). Abbreviations: N-BCAA/N-INS Normal BCAA, normal insulin.

**Figure 8.** Mouse blastocyst cell volume and correlation analyses between cell volume and endocytosis/lysosome factors for N-BCAA/N-INS (blue) and L-ILE/N-INS treatments (red). **A.** Cell volume is not significantly changed between treatment groups assayed by LysoTracker and BSA-BODIPY. **B,C.** Cell volume and LysoTracker number and collective volume, respectively, are positively and significantly correlated in N-BCAA/N-INS and L-ILE/N-INS with LysoTracker data increased in the L-ILE/N-INS group. **D,E.** Cell volume and BSA-BODIPY number and collective volume, respectively, are positively correlated in N-BCAA/N-INS and L-ILE/N-INS with BSA-BODIPY data increased in the L-ILE/N-INS group. **F.** Cell volume is not significantly changed between N-BCAA/N-INS and L-ILE/N-INS groups assayed for TFEB. **G.** No correlation was found between cell volume and the percentage of TFEB in the nucleus in both groups. Data were analysed by Kruskal-Wallis (**A**), correlation (**B-E,G**) or t test (**F**) and shown as dot plots with box and whisker markers to identify the median and interquartile range and min/max points (**A,F**) or dot plot correlation analysis (**B-E,G**). 7-8 embryos per group (9-10 cells per group) from 4 mothers (in 4 replicates). Abbreviations: N-BCAA/N-INS Normal BCAA, normal insulin; L-VAL/N-INS

947 low valine, normal insulin; L-LEU/N-INS low leucine, normal insulin; L-ILE/N-INS low
948 isoleucine, normal insulin; N-BCAA/L-INS normal BCAA, low insulin.
949
950 **Figure 9.** LysoTracker collective volume per cell in human blastocyst TE from normal and
951 high BMI patients. **A.** Top TE cells labelled with LysoTracker (LysTr, red) and DAPI; scale
952 bar = 40 μm; single TE cell analysed in VOLOCITY software; scale bar = 5μm. **B.**
953 LysoTracker volume per TE cell in blastocysts is higher for high BMI than normal BMI
954 patients. Each point is a single blastocyst and patient ID number is given alongside as in
955 **Table 2**. Mother ID was a cofactor in statistical analysis to account for possible similarity of
956 embryos from the same mother. **E,F.** Cell number and cell volume, respectively, are not
957 different between blastocysts from normal and high BMI patients. However, cell volume and
958 number were significantly influencing cofactors. Data were analysed by multilevel random
959 effects regression and shown as dot plots with mean and SEM. *P< 0.05; for other P values,
960 see text; 13-15 embryos per group from 7 mothers per group.
961
962 **Figure 10.** TE cells from human blastocysts stained with TFEB (green) and DAPI (blue)
963 from normal and high BMI patients. **A.** TFEB is mainly located in the cytoplasm in embryos
964 from normal BMI mothers while more TFEB staining co-localizes with the nucleus in high
965 BMI mothers. Scale bar = 5μm. **B.** Pearson correlation showing increased mean co-
966 localisation between TFEB and DAPI (nuclear staining) in high versus normal BMI patients
967 but not to significance. Numbers represent Patient ID from **Table 2**. **C,D.** LysoTracker
968 collective volume and TFEB nuclear co-localisation (Pearson correlation), respectively, are
969 not different when comparing embryos derived from ICSI or not. Normal (blue) and high
970 (red) BMI patients are shown. Numbers represent Patient ID from **Table 2**. Data were

971 analysed by multilevel random effects regression and shown as dot plots with mean and
972 SEM. For select P values, see text;13-14 embryos per group from 7 mothers per group.
973
974 **Supplemental Figure 1.** Mouse blastocyst LysoTracker (**A, C**) and BSA-BODIPY (**B, D**)
975 individual vesicle volumes and their distance from nucleus were not altered in response to
976 different culture treatments. Embryos were cultured from 2-cell stage and analysed at
977 blastocyst stage. **A, B.** Mean vesicle volume did not differ between groups. **C, D.** Mean
978 vesicle distance to nucleus did not differ between groups. **E.** Percentage (%) of embryos
979 developing to blastocysts following culture from 2-cell stage after 48 h did not differ between
980 treatments. **F.** Cell number in blastocysts did not differ between treatments. Data were
981 analysed by Kruskal-Wallis (**A,C,E**) or 1-way ANOVA (**B,D,F**) and shown as dot plots with
982 box and whisker markers to identify the median and interquartile range and min/max points.
983 17-24 embryos per group (30-55 cells per group) from 13 mothers (in 10 replicates).
984
985 **Supplemental Figure 2.** Mouse blastocyst LysoTracker (**A,C**) and BSA-BODIPY (**B,D**)
986 individual vesicle volumes and their distance from nucleus were not altered in response to
987 different culture treatments. Embryos were cultured from 2-cell stage and analysed at
988 blastocyst stage. **A,B.** Mean vesicle volume did not differ between groups. **C,D.** Mean vesicle
989 distance to nucleus did not differ between groups. Data were analysed by 1-way ANOVA and
990 shown as dot plots with box and whisker markers to identify the median and interquartile
991 range and min/max points. 13-19 embryos per group (23-38 cells per group) from 14 mothers
992 (in 8 replicates).
993

**Table 1**. Amino acid concentrations present *in vivo* in the NPD mother uterine fluid at E3.5 (Eckert et al., 2012) and used in the N-BCA medium.

| **AMINO ACIDS** | Concentration (mM) |
|---|---|
| Alanine | 3.8 |
| Arginine | 0.16 |
| Asparagine | 0.14 |
| Aspartic acid | 1.83 |
| Glutamic acid | 4.72 |
| Glutamine | 1.41 |
| Glycine | 2.68 |
| Histidine | 0.14 |
| Isoleucine | 0.21 |
| Leucine | 0.32 |
| Lysine | 0.5 |
| Methionine | 0.18 |
| Phenylalanine | 0.14 |
| Serine | 0.97 |
| Taurine | 14.74 |
| Threonine | 0.72 |
| Tryptophan | 0.06 |
| Tyrosine | 0.18 |
| Valine | 0.45 |

**Table 2**. Patient and human embryo criteria, **A** Normal BMI; **B** High BMI. ICSI, intracytoplasmic sperm injection. Condition: PCOS, polycystic ovary syndrome; Low S+O, low sperm and ovarian reserve; Male Inf, male infertility; Unexpl, unexplained; Tubal, tubal blockage.

| **A** | **Normal BMI** | | | | | | | |
|---|---|---|---|---|---|---|---|---|
| | **Patient 1** | **Patient 2** | **Patient 3** | **Patient 4** | **Patient 5** | **Patient 6** | **Patient 7** | **Mean** |
| **BMI** | 18.97 | 21.72 | 22.94 | 21.91 | 23.1 | 22.48 | 22.14 | 21.90 |
| **Age** | 31 | 35 | 27 | 38 | 33 | 35 | 35 | 33.75 |
| **Condition** | PCOS | Low S+O | Male Inf | Unexpl | Male Inf | Tubal | Unexpl | |
| **Number embryos** | 8 | 3 | 10 | 7 | 4 | 6 | 4 | Total 42 |
| **Stage stored** | D3 | D3 (2)<br>D5 (1) | D3 | D5 | D3 | D3 (3)<br>D5 (3) | D5 | |
| **ICSI** | NO | YES | YES | NO | YES | NO | NO | 5 NO / 3 YES |
| **Pregnancy that cycle** | YES | NO | NO | YES | YES | NO | YES | 3 NO /5 YES |
| **Blastocysts formed** | 3 | 1 | 3 | 3 | 1 | 2 | 2 | Total 15 (36%) |

| **B** | **High BMI** | | | | | | | |
|---|---|---|---|---|---|---|---|---|
| | **Patient 8** | **Patient 9** | **Patient 10** | **Patient 11** | **Patient 12** | **Patient 13** | **Patient 14** | **Mean** |
| **BMI** | 32.39 | 31.25 | 31.16 | 30.12 | 27.25 | 27.15 | 29.76 | 29.54 |
| **Age** | 36 | 35 | 34 | 35 | 34 | 36 | 35 | 34.7 |
| **Condition** | PCOS +<br>Male Inf | Unexpl | Tubal +<br>Male Inf | Unexpl | PCOS | Tubal | PCOS | |
| **Number embryos** | 4 | 4 | 4 | 7 | 9 | 8 | 3 | Total 39 |
| **Stage stored** | D4 (2)<br>D5 (2) | D3 | D3 | D3 | D3 (7)<br>D5(2) | D3 (6)<br>D5 (2) | D3 | |
| **ICSI** | YES | YES | YES | YES | NO | NO | YES | 4 NO / 5 YES |
| **Pregnancy that cycle** | YES | YES | YES | NO | YES | YES | NO | 7 YES / 2 NO |
| **Blastocysts formed** | 1 | 1 | 2 | 3 | 4 | 3 | 2 | Total 16 (41%) |

**Supplementary Table 1**. VOLOCITY protocols used for quantitative image analysis.

**(a) LysoTracker or MagicRed™ and BSA-BODIPY analysis**

1. Crop cell
2. Find object (based on channel) – red channel for LysoTracker Red or MagicRed™; green channel for BSA-BODIPY; blue channel (DAPI – nucleus)
3. Remove noise from objects (fine filter)
4. Separate touching objects (by 2 μm)
5. Exclude objects by size: chosen based on the literature, according to Tsichlaki and Fitzharris, (2016) the blastocyst nuclei size is 690±20 $\mu m^3$ while the lysosome size range is between 0.1 – 1.2 μm diameter (Kuehnel, 2003)
   5.1. vesicles <0.01 $\mu m^3$ and > 20 $\mu m^3$
   5.2. nuclei < 150 $\mu m^3$
6. Nuclei – fill holes in objects
7. Objects of interest were selected by automatic threshold using an offset of 50%.
8. Measure distance from vesicle centre to nucleus edge (TE).
9. Object data were exported to Excel for analysis.

**(b) TFEB analysis**

1. Crop cell
2. Find object (based on channel) – blue channel (DAPI – nucleus) and green channel for TFEB
3. Remove noise from objects (fine filter)
4. Separate touching objects (by 2 μm)
5. Exclude objects by size: chosen based on the literature, according to Tsichlaki and Fitzharris, (2016) the blastocyst nuclei size is 690±20 $\mu m^3$
   5.1. nuclei < 150 $\mu m^3$Nuclei – fill holes in objects
6. Objects of interest were selected by automatic threshold using an offset of 50%.
7. Define cytoplasm: subtract nucleus from ROIs (cell)
8. Find TFEB in nucleus: intersect nucleus with TFEB
   8.1. Remove noise from objects (fine filter)
   8.2. Separate touching objects (by 2 μm)
9. Find TFEB in cytoplasm: intersect cytoplasm with TFEB
   9.1. Remove noise from objects (fine filter)

9.2. Separate touching objects (by 2 μm)

10. Colocalization: automatic threshold (Costes) – Costes Pearson correlation
11. Object data were exported to Excel for analysis.

# Figure 1

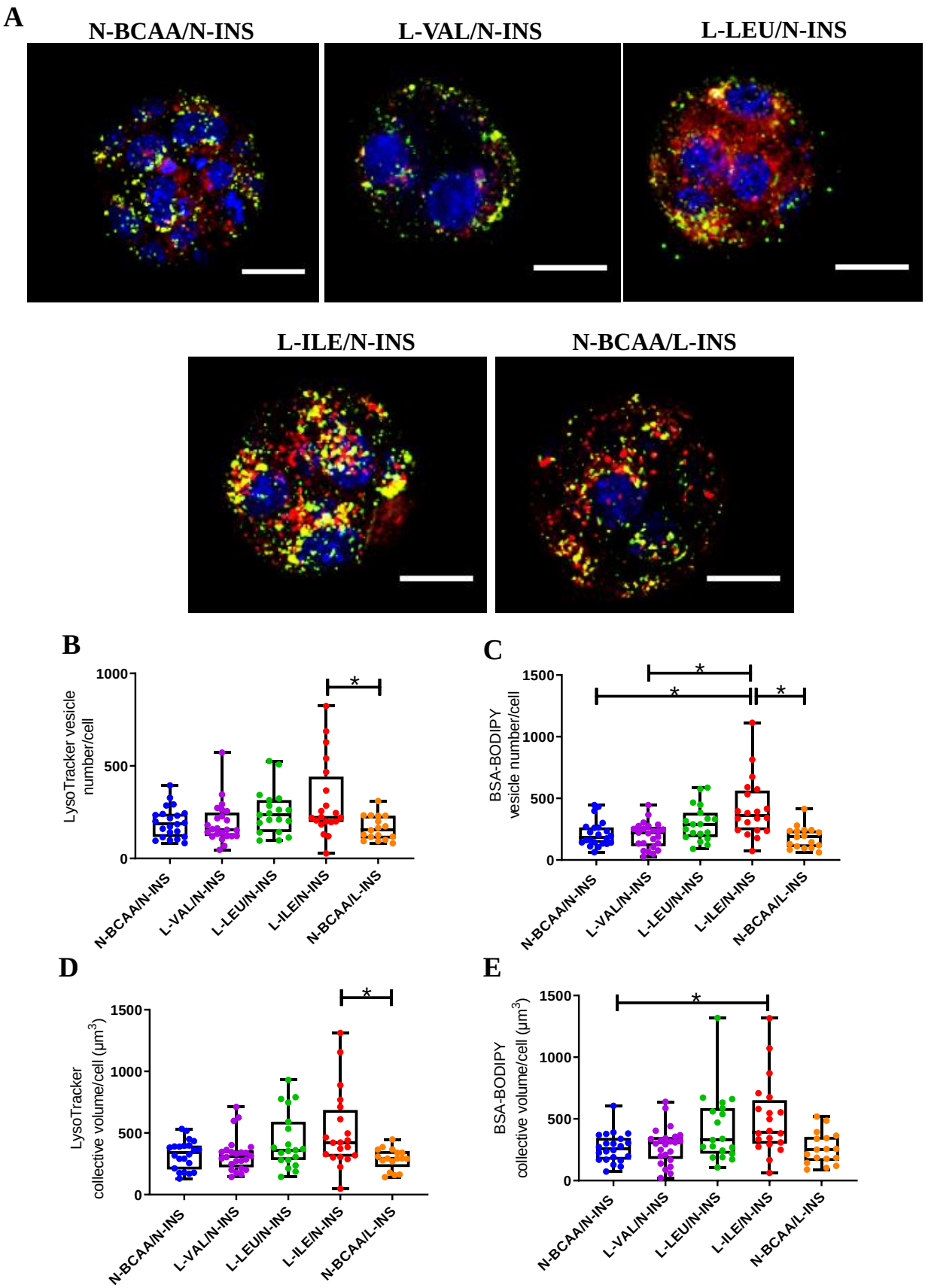
A
N-BCAA/N-INS
L-VAL/N-INS
L-LEU/N-INS
L-ILE/N-INS
N-BCAA/L-INS
B
LysoTracker vesicle number/cell
1000
500
0
*
N-BCAA/N-INS
L-VAL/N-INS
L-LEU/N-INS
L-ILE/N-INS
N-BCAA/L-INS
C
BSA-BODIPY vesicle number/cell
1500
1000
500
0
*
*
*
N-BCAA/N-INS
L-VAL/N-INS
L-LEU/N-INS
L-ILE/N-INS
N-BCAA/L-INS
D
LysoTracker collective volume/cell (µm3)
1500
1000
500
0
*
N-BCAA/N-INS
L-VAL/N-INS
L-LEU/N-INS
L-ILE/N-INS
N-BCAA/L-INS
E
BSA-BODIPY collective volume/cell (µm3)
1500
1000
500
0
*
N-BCAA/N-INS
L-VAL/N-INS
L-LEU/N-INS
L-ILE/N-INS
N-BCAA/L-INS

# Figure 2

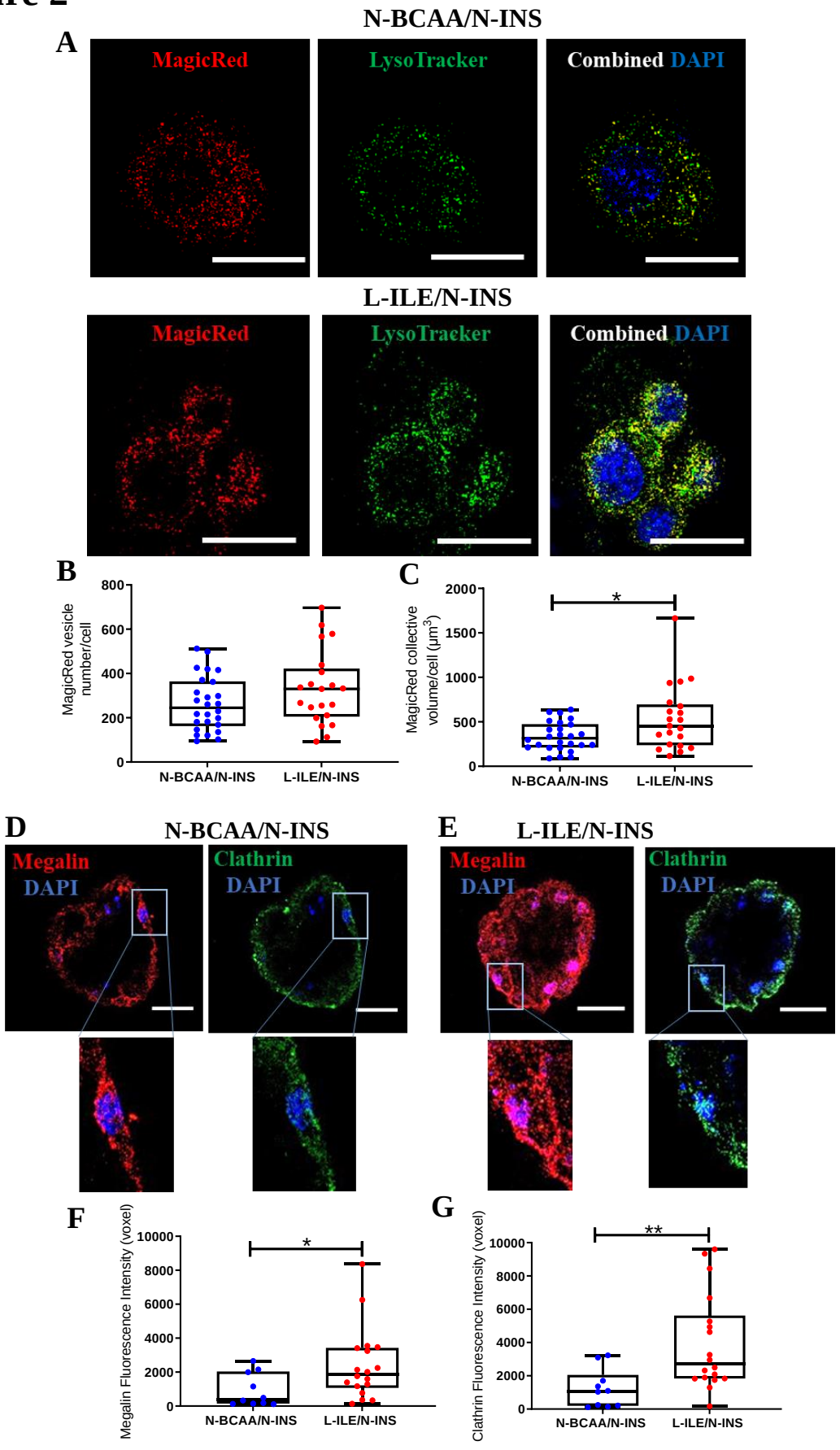
A
N-BCAA/N-INS
MagicRed
LysoTracker
Combined DAPI
L-ILE/N-INS
MagicRed
LysoTracker
Combined DAPI
B
MagicRed vesicle number/cell
800
600
400
200
0
N-BCAA/N-INS
L-ILE/N-INS
C
MagicRed collective volume/cell (μm3)
2000
1500
1000
500
0
*
N-BCAA/N-INS
L-ILE/N-INS
D
N-BCAA/N-INS
Megalin
DAPI
Clathrin
DAPI
E
L-ILE/N-INS
Megalin
DAPI
Clathrin
DAPI
F
Megalin Fluorescence Intensity (voxel)
10000
8000
6000
4000
2000
0
*
N-BCAA/N-INS
L-ILE/N-INS
G
Clathrin Fluorescence Intensity (voxel)
10000
8000
6000
4000
2000
0
**
N-BCAA/N-INS
L-ILE/N-INS

# Figure 3

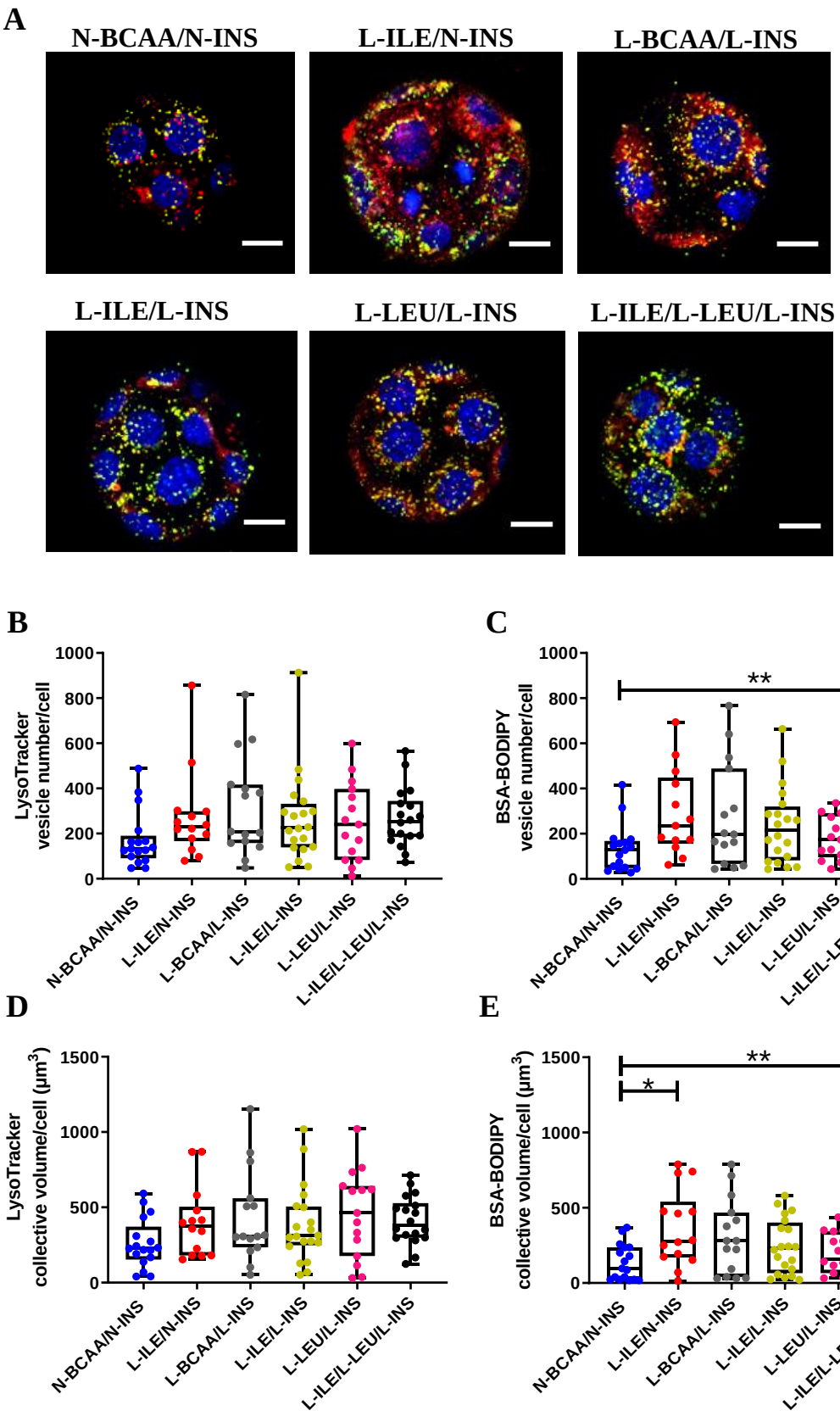
A
N-BCAA/N-INS
L-ILE/N-INS
L-BCAA/L-INS
L-ILE/L-INS
L-LEU/L-INS
L-ILE/L-LEU/L-INS
B
LysoTracker vesicle number/cell
1000
800
600
400
200
0
N-BCAA/N-INS
L-ILE/N-INS
L-BCAA/L-INS
L-ILE/L-INS
L-LEU/L-INS
L-ILE/L-LEU/L-INS
C
BSA-BODIPY vesicle number/cell
**
D
LysoTracker collective volume/cell (µm3)
1500
1000
500
0
E
BSA-BODIPY collective volume/cell (µm3)
*
**

# Figure 4

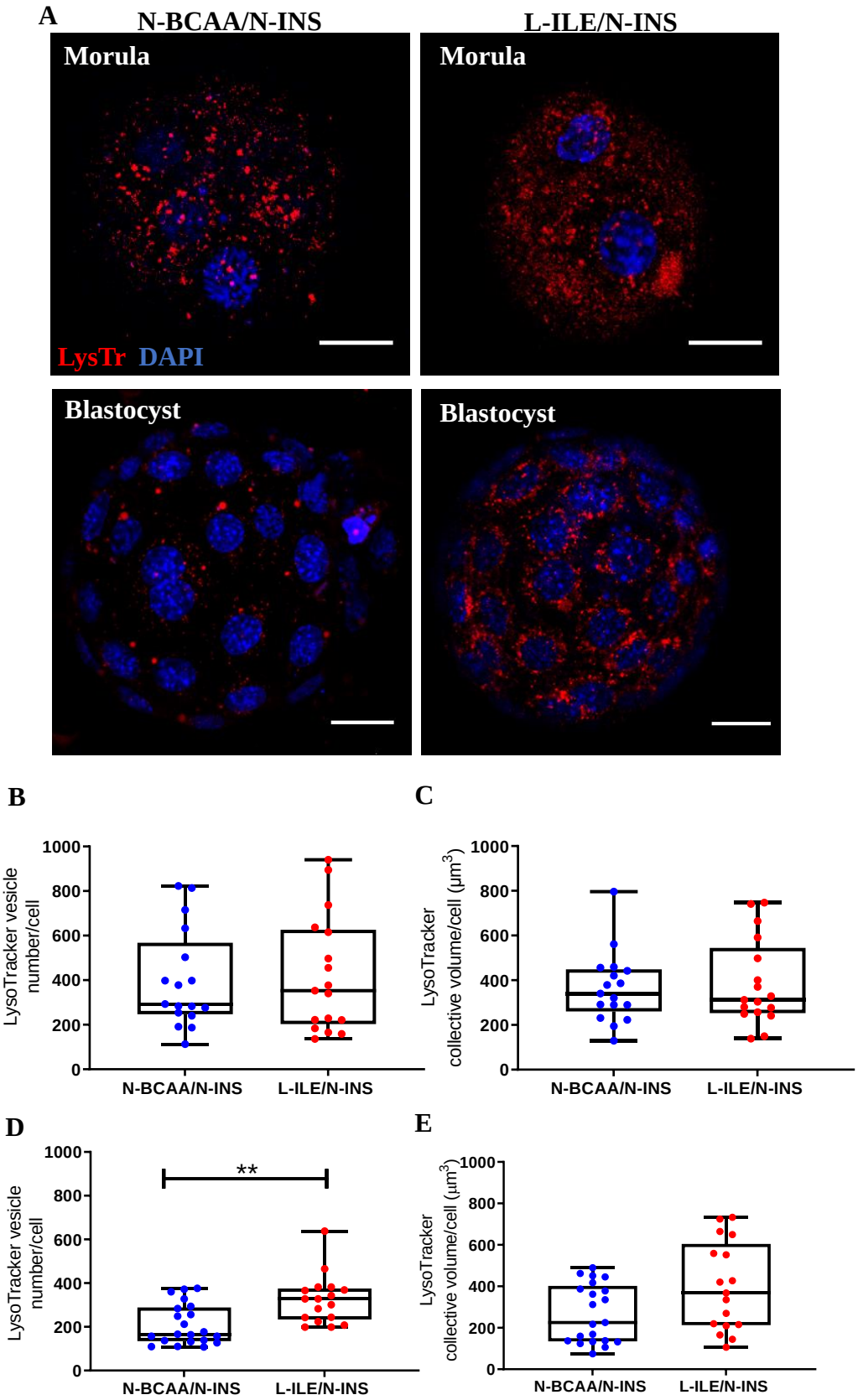
A
N-BCAA/N-INS
L-ILE/N-INS
Morula
Morula
LysTr DAPI
Blastocyst
Blastocyst
B
LysoTracker vesicle number/cell
1000
800
600
400
200
0
N-BCAA/N-INS
L-ILE/N-INS
C
LysoTracker collective volume/cell (μm3)
1000
800
600
400
200
0
N-BCAA/N-INS
L-ILE/N-INS
D
LysoTracker vesicle number/cell
**
1000
800
600
400
200
0
N-BCAA/N-INS
L-ILE/N-INS
E
LysoTracker collective volume/cell (μm3)
1000
800
600
400
200
0
N-BCAA/N-INS
L-ILE/N-INS

# Figure 5

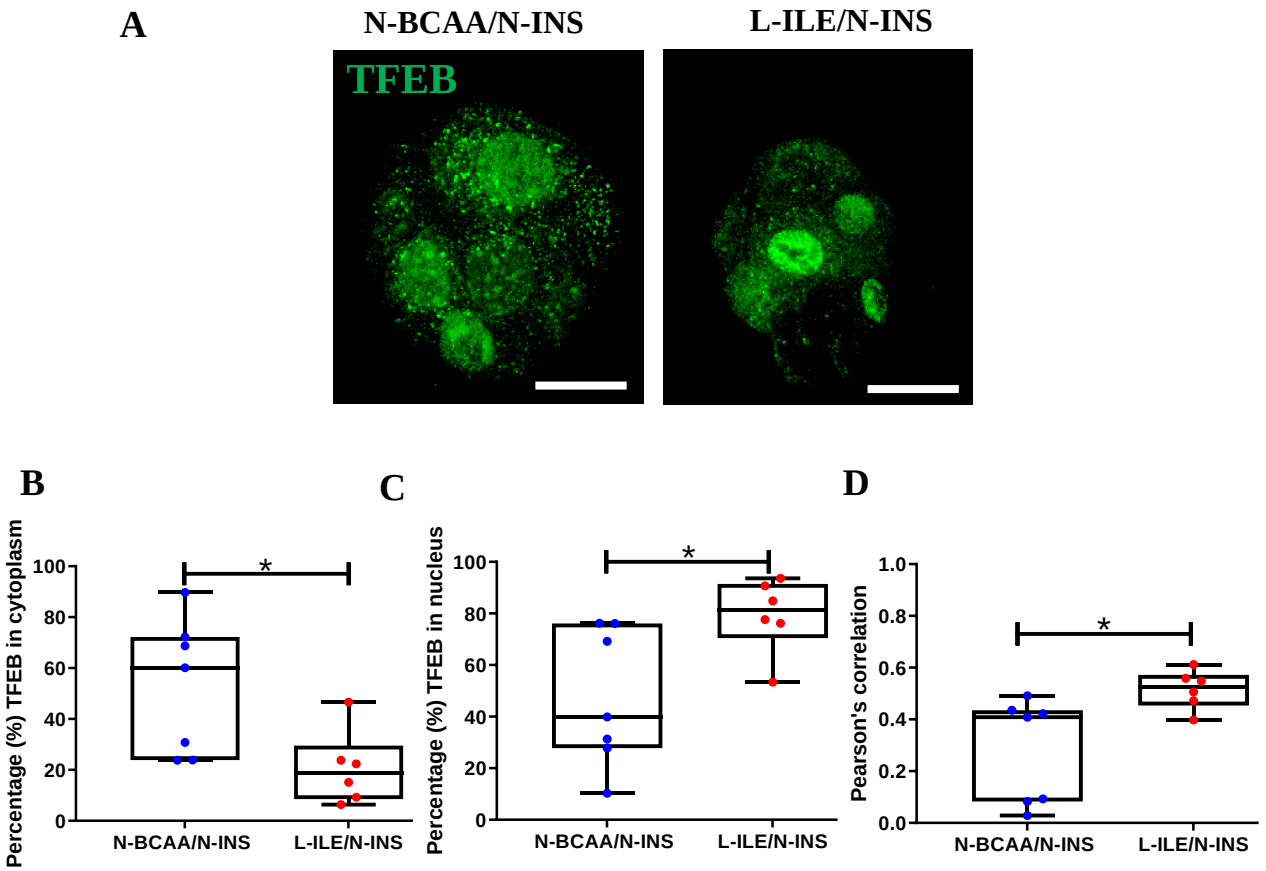
A
N-BCAA/N-INS
L-ILE/N-INS
TFEB
B
Percentage (%) TFEB in cytoplasm
100
80
60
40
20
0
*
N-BCAA/N-INS
L-ILE/N-INS
C
Percentage (%) TFEB in nucleus
100
80
60
40
20
0
*
N-BCAA/N-INS
L-ILE/N-INS
D
Pearson's correlation
1.0
0.8
0.6
0.4
0.2
0.0
*
N-BCAA/N-INS
L-ILE/N-INS

# Figure 6

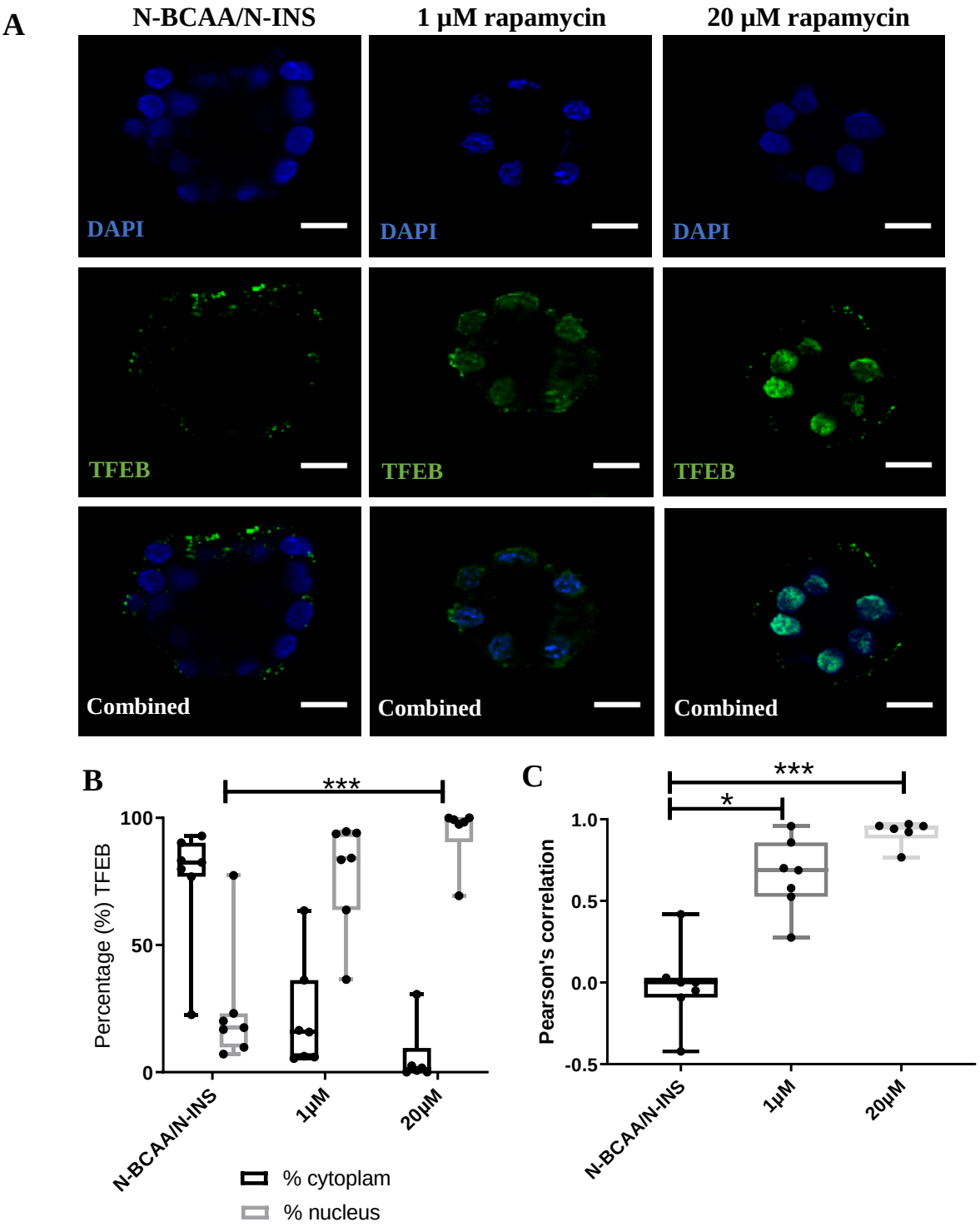
A
N-BCAA/N-INS
1 μM rapamycin
20 μM rapamycin
DAPI
TFEB
Combined
B
***
Percentage (%) TFEB
100
50
0
N-BCAA/N-INS
1μM
20μM
% cytoplam
% nucleus
C
***
*
Pearson's correlation
1.0
0.5
0.0
-0.5
N-BCAA/N-INS
1μM
20μM

# Figure 7

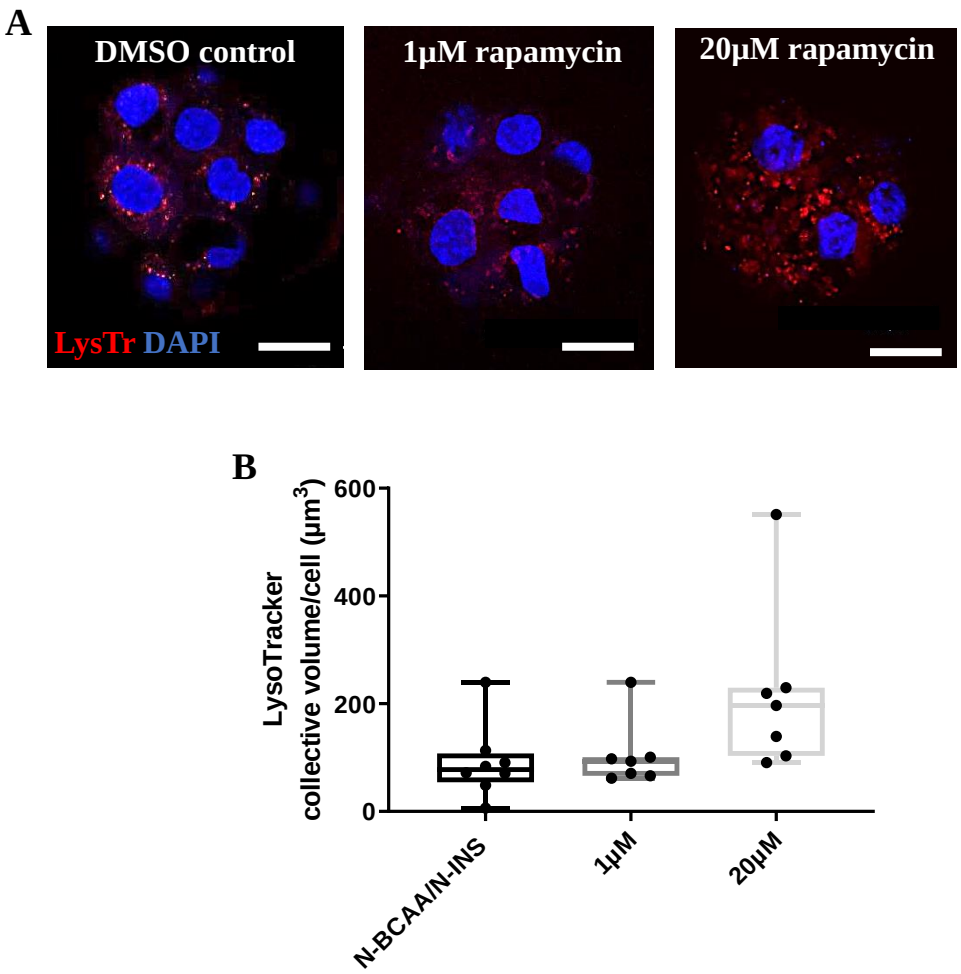
A
DMSO control
1µM rapamycin
20µM rapamycin
LysTr DAPI
B
LysoTracker collective volume/cell (µm3)
600
400
200
0
N-BCAA/N-INS
1µM
20µM

# Figure 8

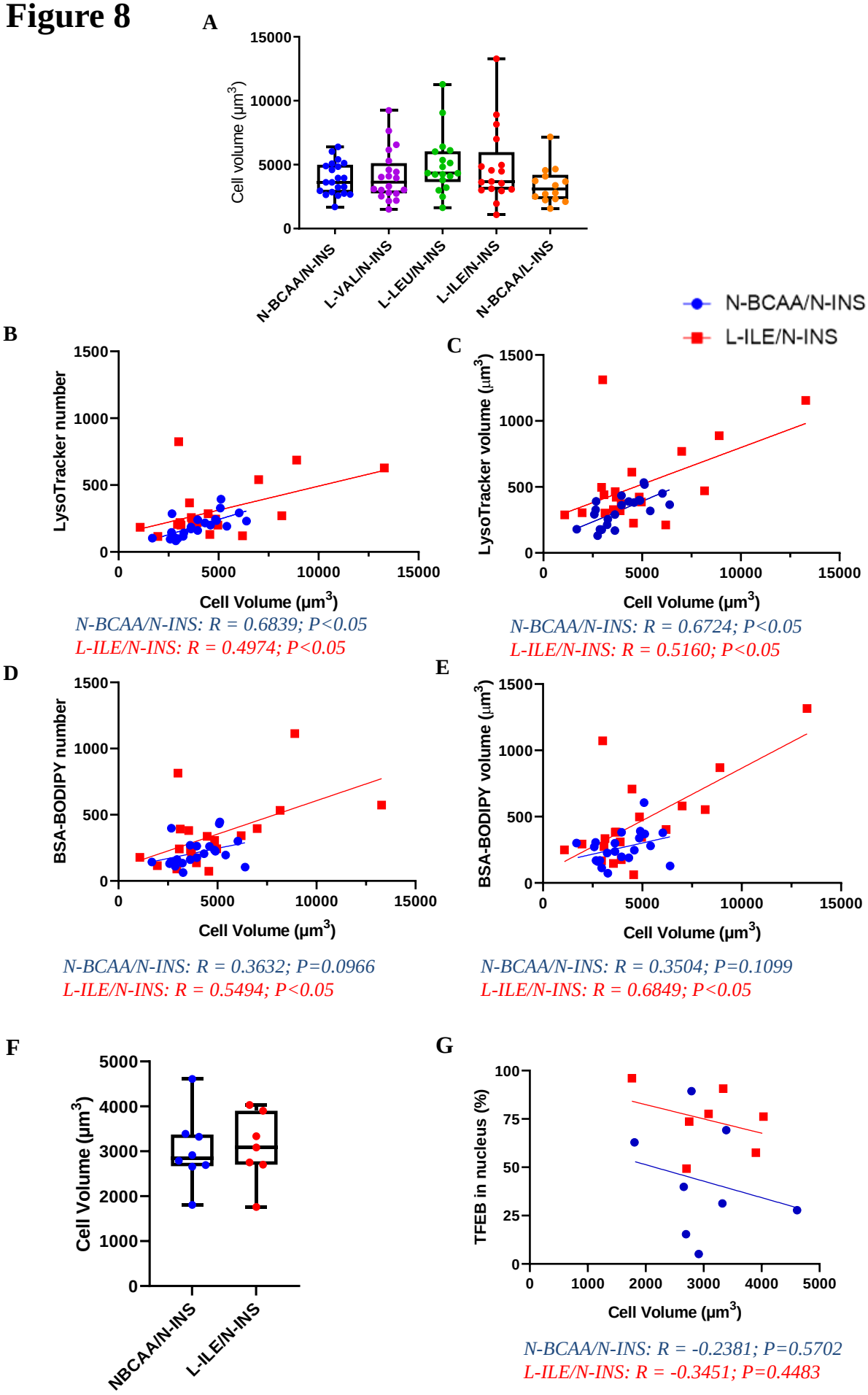
A
Cell volume (µm3)
15000
10000
5000
0
N-BCAA/N-INS
L-VAL/N-INS
L-LEU/N-INS
L-ILE/N-INS
N-BCAA/L-INS
N-BCAA/N-INS
L-ILE/N-INS
B
LysoTracker number
Cell Volume (µm3)
N-BCAA/N-INS: R = 0.6839; P<0.05
L-ILE/N-INS: R = 0.4974; P<0.05
C
LysoTracker volume (µm3)
Cell Volume (µm3)
N-BCAA/N-INS: R = 0.6724; P<0.05
L-ILE/N-INS: R = 0.5160; P<0.05
D
BSA-BODIPY number
Cell Volume (µm3)
N-BCAA/N-INS: R = 0.3632; P=0.0966
L-ILE/N-INS: R = 0.5494; P<0.05
E
BSA-BODIPY volume (µm3)
Cell Volume (µm3)
N-BCAA/N-INS: R = 0.3504; P=0.1099
L-ILE/N-INS: R = 0.6849; P<0.05
F
Cell Volume (µm3)
5000
4000
3000
2000
1000
0
NBCAA/N-INS
L-ILE/N-INS
G
TFEB in nucleus (%)
100
75
50
25
0
Cell Volume (µm3)
N-BCAA/N-INS: R = -0.2381; P=0.5702
L-ILE/N-INS: R = -0.3451; P=0.4483

# Figure 9

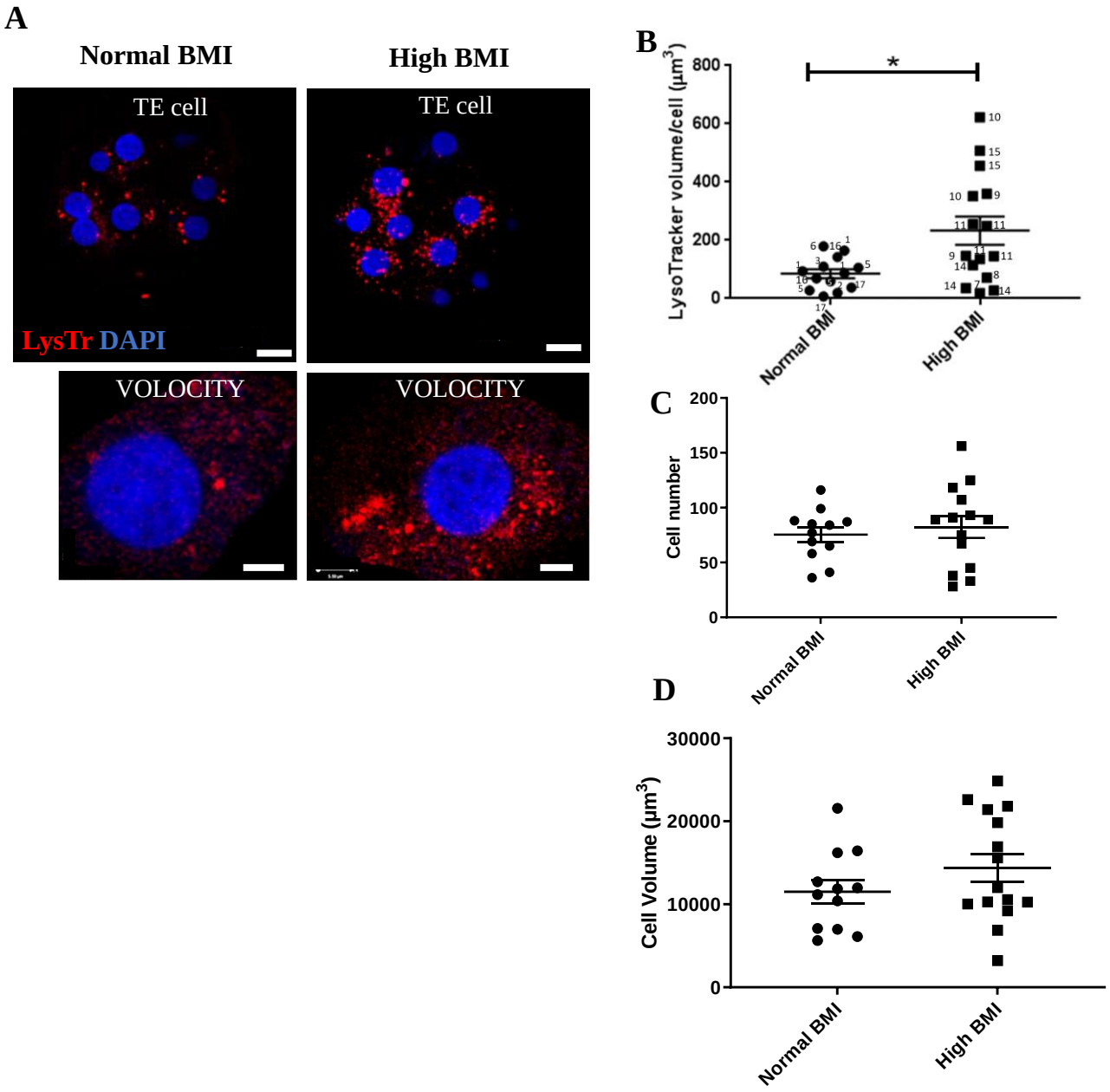
A
Normal BMI
High BMI
TE cell
TE cell
LysTr DAPI
VOLOCITY
VOLOCITY
B
LysoTracker volume/cell (µm3)
800
600
400
200
0
*
Normal BMI
High BMI
C
Cell number
200
150
100
50
0
Normal BMI
High BMI
D
Cell Volume (µm3)
30000
20000
10000
0
Normal BMI
High BMI

# Figure 10

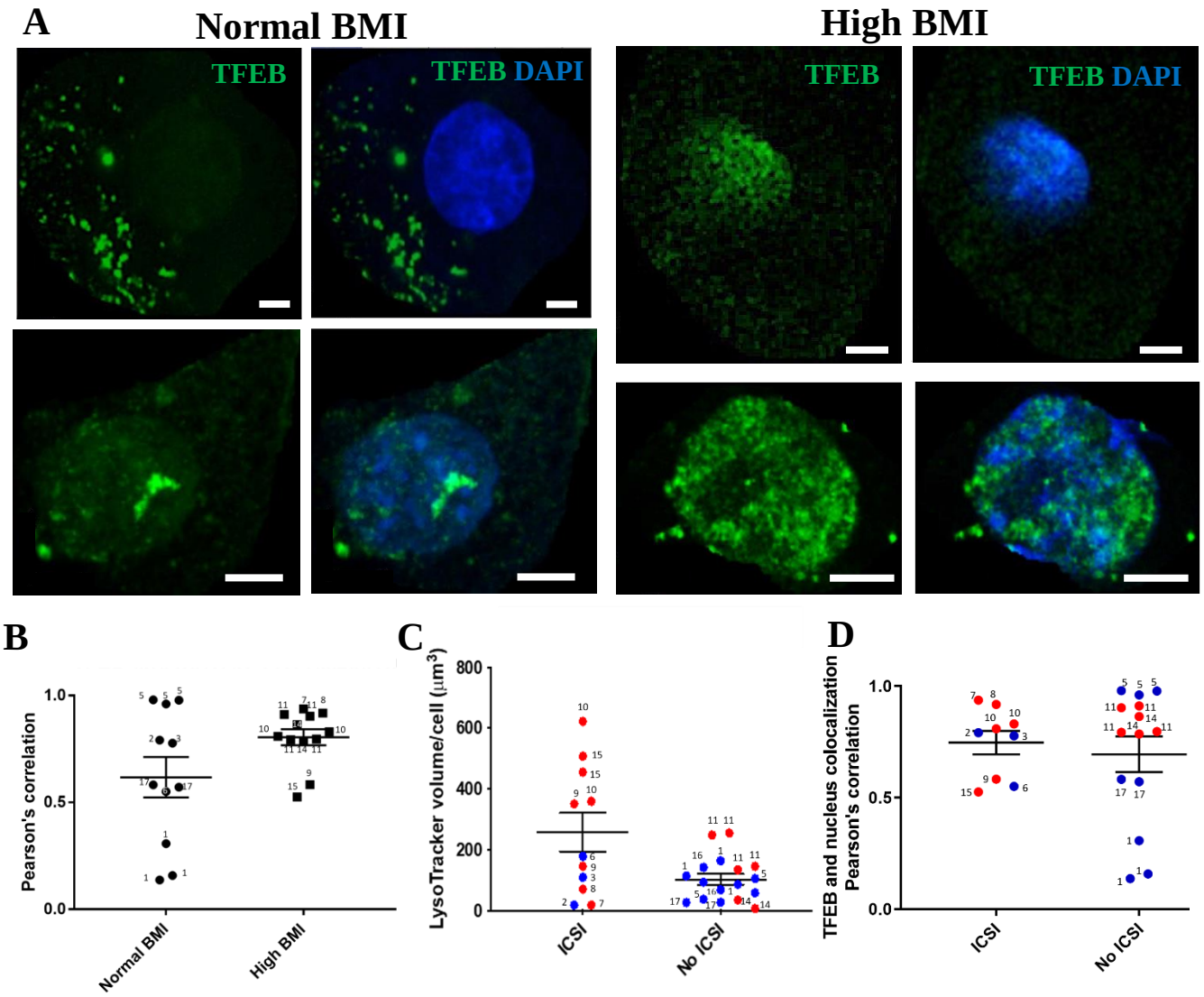
A
Normal BMI
High BMI
TFEB
TFEB DAPI
TFEB
TFEB DAPI
B
Pearson's correlation
1.0
0.5
0.0
Normal BMI
High BMI
C
LysoTracker volume/cell (μm3)
800
600
400
200
0
ICSI
No ICSI
D
TFEB and nucleus colocalization
Pearson's correlation
1.0
0.5
0.0
ICSI
No ICSI

# Supplementary Figure 1

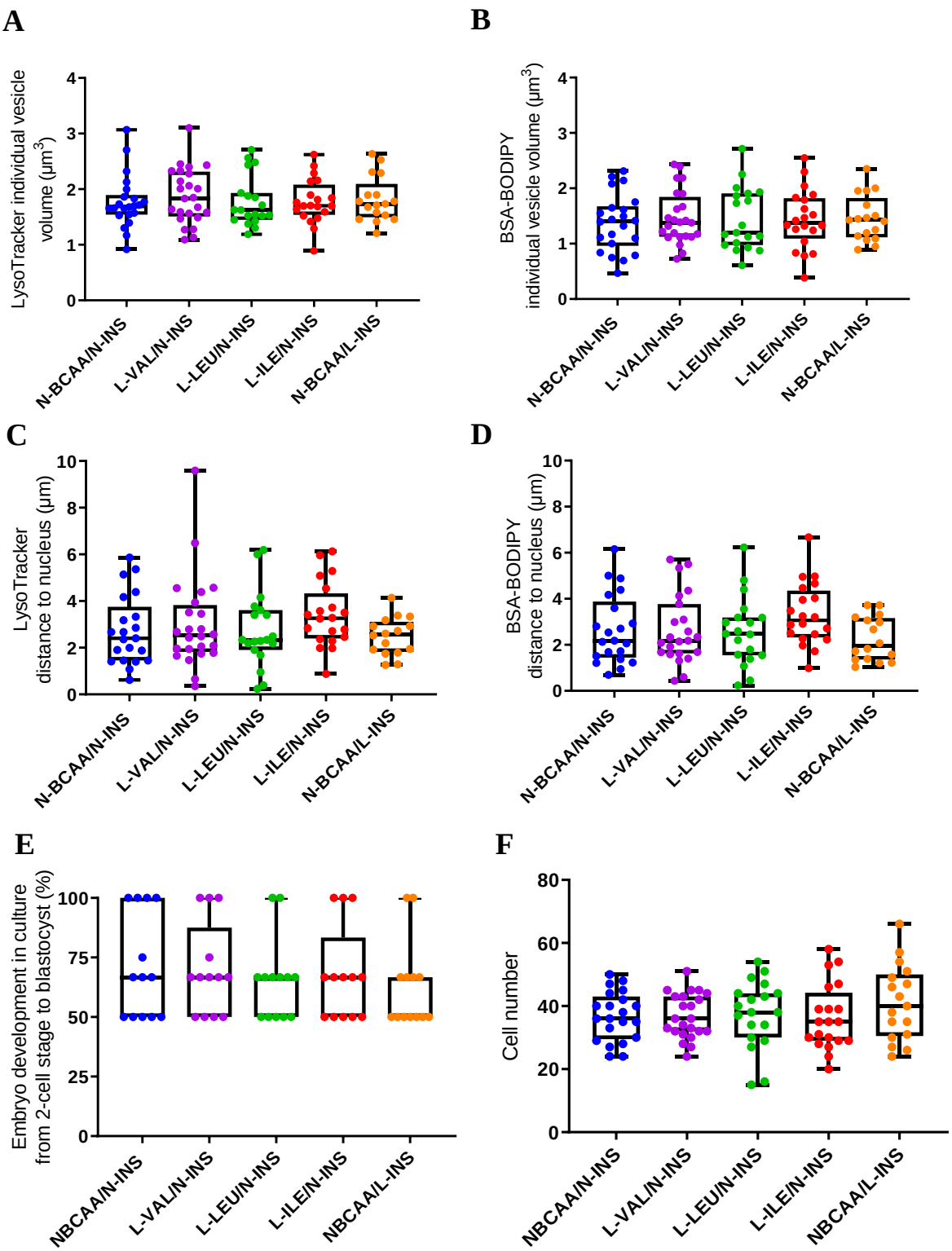

# Supplementary Figure 2